TRACTION ESTIMATION AND CONTROL FOR MOBILE ROBOTS USING WHEEL SLIP VELOCITY

JARED D. TERRY

TRACTION ESTIMATION AND CONTROL FOR MOBILE ROBOTS USING WHEEL SLIP VELOCITY

by

Jared D. Terry

A thesis submitted to the faculty of
The University of Utah
in partial fulfillment of the requirements for the degree of

Master of Science

Department of Mechanical Engineering

University of Utah

December 2008

THE UNIVERSITY OF UTAH GRADUATE SCHOOL

SUPERVISORY COMMITTEE APPROVAL

of a thesis submitted by

Jared D. Terry

This thesis has been read by each member of the following supervisory committee and by majority vote has been found to be satisfactory.

5/28/2008 — Chair: Mark A. Minor

5/29/08 — John Hollerbach

5/29/2008 — Eric Pardyjak

THE UNIVERSITY OF UTAH GRADUATE SCHOOL

FINAL READING APPROVAL

To the Graduate Council of the University of Utah:

I have read the thesis of Jared D. Terry in its final form and have found that (1) its format, citations, and bibliographic style are consistent and acceptable; (2) its illustrative materials including figures, tables, and charts are in place; and (3) the final manuscript is satisfactory to the supervisory committee and is ready for submission to The Graduate School.

5/29/2008
Date

Mark A. Minor
Chair: Supervisory Committee

Approved for the Major Department

Kent S. Udell
Chair/Dean

Approved for the Graduate Council

David S. Chapman
Dean of The Graduate School

ABSTRACT

Mobile robots are used to venture through types of environments, at low wheel speeds, where wheel slip is a threat. Wheel slip is a hazard to mobile robots in that it introduces error in dead reckoning measurement and in some instances causes the robot to halt its forward progress. To compensate for traction loss several methods are used to determine the terrain characteristics. One of these methods is Pacejka's Tire Model. The slope of Pacejka's Tire Model can be used to determine when traction loss occurs.

One step toward realizing the slope of Pacejka's Tire Model is achieving a good estimate of wheel slip. We present a unique traction estimation algorithm for low speed applications that estimates traction loss by measuring the wheel slip velocity by coupling the dynamics of a wheel with the dynamics of a vehicle. Estimates of the wheel slip velocity are accomplished using onboard sensors. To obtain an accurate estimate of the wheel slip velocity, we propose a modified Kalman Filter that fuses a system model of a DC motor with an estimate of the disturbances acting on the system model. Using the wheel slip velocity a neighborhood can be defined between two instances in time that estimates when traction loss occurs.

With means of estimating traction loss, we propose a traction control law for low speed applications that provides the ability of tracking a desired reference while mitigating traction loss. To solve the tracking problem we propose a robust tracking controller that provides the ability of following a defined path and rejecting unmodeled

disturbances. To mitigate traction loss we propose a continuous robust traction controller to maximize traction forces by containing wheel slip and its derivative to a neighborhood. The unique aspect of our traction controller is it works jointly with our proposed tracking controller.

I dedicate this thesis to my father, Courtney Dixon Terry, whose has always inspired me to rise above mediocrity, and whose wisdom, love, and guidance has always been there to pull me up when I have stumbled.

TABLE OF CONTENTS

LIST OF TABLES

Table Page

LIST OF FIGURES

ACKNOWLEDGMENTS

I would like to thank Dr. Mark A. Minor for his patience, guidance, and leadership, Jill Terry for her love, support, and dedication, and Karen Hayes and Courtney Terry for assisting me in proof reading my thesis.

1. INTRODUCTION

Traction is simply the contact force between a rolling wheel and the ground upon which it is rolling. Often in vehicle dynamics, traction is considered to be ideal, which means that a vehicle is in a state of pure rolling without slip. The relative ground speed, ω/r, therefore, equates to the linear velocity, v, of the vehicle, Figure 1a. In this ideal state of perfect traction the force applied by the wheel, F_T, produces a translational force, F, on the vehicle. Both [1] and [2] simplify their kinematic model by assuming their robot is under the constraint of pure rolling without slip. When the traction force, however, is unable to compensate for the force applied by the wheel, the relative ground velocity is faster than the linear velocity of the vehicle, Figure 1b. Wheel slip, therefore, is occurring. The force applied by the wheel therefore does not map perfectly to the translational force of the vehicle. This is known as traction loss. Traction often is not modeled in vehicle dynamics due to its nonlinear behavior. Recent advances in the automotive and the mobile robot communities, however, suggest a need for the development of control laws capable of mitigating traction loss.

To increase the safety of automobiles, the automotive industry has developed vehicles with anti-lock braking systems (ABS) and traction control systems (TCS). ABS has been incorporated on vehicles to remove the ability of the breaks to lock. An ABS modulates the hydraulic pressure applied to the brake calipers in order to maintain optimal rotor slip. By sustaining optimal rotor slip provides the necessary amount of

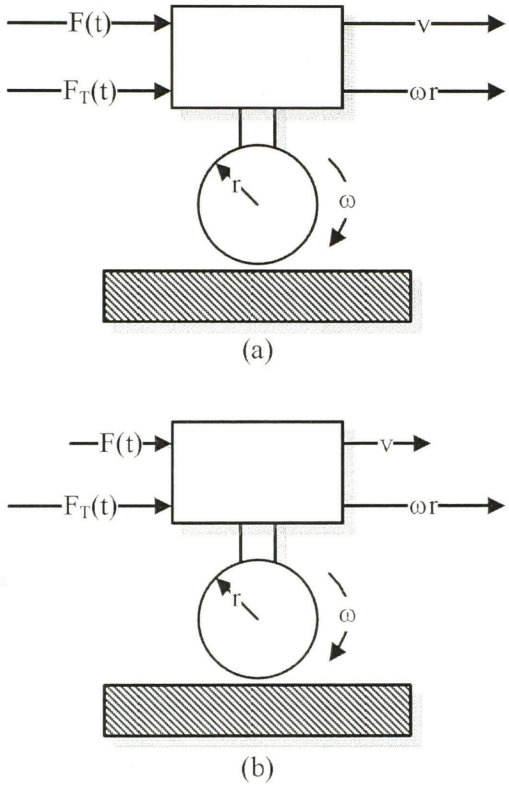

Figure 1: Effects of traction force on a vehicle (a) pure rolling without slip, (b) rolling with slip

braking torque to effectively reduce the speed of a vehicle. ABS, therefore, allows defensive maneuvers to be accomplished without loosing control of the vehicle. The application of ABS has given rise to traction control systems.

Traction control systems mitigate the effects of traction loss by maintaining optimal wheel slip. Optimal wheel slip is achieved by providing a vehicle with the capability of controlling the vehicle's wheel speed. By controlling the wheel speed the relative ground velocity approaches that of the linear velocity of the vehicle. In other words, the error between the relative ground velocity and the linear velocity approaches zero. As the error between the relative ground velocity and the linear velocity is reduced the vehicle maintains the proper amount of traction to steer the vehicle. Traction control systems are therefore ideal for acceleration and cornering on hazardous roads and environments.

Mitigation of traction loss has also been a growing area of interest in the arena of mobile robots. Iagnemma and Dubowsky [3] expressed their interests in using mobile robots for planetary missions. They argue that these planetary expeditions contain rough to benign terrain, which complicates the ability to navigate. To navigate through these terrains with a high level of confidence, they propose motion planning architecture, which mitigates traction loss. Mobile robots, however, are not confined solely to planetary expeditions, but are often designed to travel in environments where there is a high risk to human safety. Often in these environments the mobile robot is required to travel across difficult terrain. Some of these environments may be a disaster site, a mining tunnel, or a sewer system. Though both the automotive and mobile robot communities express interest in traction control systems, there are differences in their

application. One of the differences in the application of traction control systems is that, typically, mobile robots are constrained to lower speeds.

Due to the environments that mobile robots have been proposed to operate in, it is ideal to keep speed of the mobile robot within limitations of the environment. In conventional traction control algorithms wheel slip is used as a primary variable to quantify when traction loss is occurring. Using wheel slip, however, is prone to error when the magnitude of the linear velocity and wheel speed are small. For low speed applications an alternate parameter appears to be required to mitigate the effects of traction loss.

To mitigate the effects of traction loss for low speed applications, we propose an alternate parameter, wheel slip velocity. We also propose that the wheel slip velocity can be determined from a data fusion algorithm outlined in this thesis. The underlying foundation of our data fusion algorithm is based upon the derivative of Pacejka's Tire Model [4]. The derivative of this tire model can be used to define regions where traction is available or being lost. Our method, however, does not provide the ability, at this time, of estimating the derivative of Pacejka's Tire Model but provides an estimate of the wheel slip velocity and wheel slip acceleration. Having an estimate of the wheel slip velocity is a necessary evolutionary step towards having the ability to estimate the derivative of the slip curve for low speed applications. Using an estimate of the wheel slip velocity and the wheel slip acceleration, a neighborhood can be defined where traction loss is occurring. Validation of our traction estimation algorithm is provided through experimental results using a mobile robot. Experiments were conducted on multiple surfaces and a discussion outlining the performance of our traction estimation

algorithm will be given. Though we propose a traction estimation architecture designed for mobile robots, its application to rolling and walking robots is possible.

Applying our traction estimation architecture, we also propose a traction control law that provides a means of tracking a reference velocity while mitigating traction loss for low speed applications. Our control law was designed to enable a desired reference to be tracked when traction loss is not occurring. To mitigate traction loss we provide a continuous robust controller that bounds the wheel slip velocity in order to provide the necessary amount of traction to steer a vehicle at low speed. A robust controller is simply a control law that is designed to reject bounded disturbances acting on a system model. Our proposed traction control law also confines the wheel slip velocity to a defined neighborhood. To determine our control gains to maximize traction, multiple tests were conducted on a predetermined surface.

In Section 2 we investigated the traction control methodologies used in both the automobile and mobile robot communities'. We also introduce Pacejka's Tire Model, which is the traction model used in this thesis.

In Section 3 we derive the wheel slip velocity and wheel slip acceleration. We also introduce our modified Kalman Filter, which utilizes an estimate of motor disturbances to arrive at a better estimate of the wheel slip velocity. To evaluate the efficacy of the wheel slip velocity we propose a wheel speed tracking controller in order to provide repeatable wheel slip velocity experiments. The hardware and sensors used in these experiments are discussed. The results from our experiments show that the wheel slip velocity can be used to evaluate the onset of traction loss.

In Section 4 we use the wheel slip velocity to derive a robust traction controller. Implementing our proposed controller we will show that the control law is capable of bounding the wheel slip velocity. We will also show that using the wheel slip velocity out performs using wheel slip for low speed applications.

2. BACKGROUND

An architecture capable of alleviating the effects of traction loss requires the ability of fusing sensory data and using that fused data as an input to a traction controller. For conventional traction control architectures traction loss is quantified using an estimate of wheel slip. To ascertain the wheel slip it is required to estimate the wheel speed and the linear velocity. With the wheel speed and the linear velocity being measured parameters, their output is perturbed by noise inherited from the sensor. For an estimate of wheel speed encoders are used whose perturbed output is a function of wheel speed and sampling rate. Inertial measurement units (IMU's) are used to estimate the three axis acceleration and angular rates. The velocity measurement, however, is prone to error from drift resulting from bias and gravity. To alleviate measurement error of the angular and linear velocity observers have been designed to acquire a better estimate of these parameters. An observer is a set of linear differential equations that fuse sensory data in order to acquire a better estimate of the states of the linear differential equation.

Unsal et al. [5] designed an Extended Kalman Filter (EKF) and a sliding mode observer to estimate the wheel speed and the linear velocity of a vehicle. Estimating the wheel speed and the linear velocity enabled them to gain a better estimate of wheel slip. In comparing the two types of observers, they argued that the sliding mode observer was able to estimate the wheel slip better than the EKF since the sliding mode observer was able to compensate for the nonlinear behavior of the traction slip curve. They concluded,

however, that their sliding mode observer was unable to compensate for large deviations in the traction slip curve since the error bound on the traction slip curve was small. Buckholtz [6] incorporated an estimate of the linear acceleration to determine the brake torque for an ABS system, but never explained how they obtained the estimate.

Depending on the traction model used, other parameters, besides the wheel slip, are required to be estimated by an observer. Using the Lugre traction model, Horwitz [7] proposed an observer for tire contact friction using only the angular velocity. Their observer captured the change in road characteristics by estimating the viscous friction and a parameter used in the LuGre Model. Kango et al. [8] proposed a linear observer to estimate the load torque for ABS control. To estimate the terrain characteristics, Iagnemma and Dubowsky [3] designed an EKF to estimate the wheel contact angle. Having a better estimate the sensed parameters increased the performance of a proposed controller, which mitigates the effects of traction loss.

Traction control algorithms have been proposed in both the automotive and mobile robot communities in order to mitigate traction loss by reducing the wheel torque. Their controller designs differ in their abilities of reducing wheel torque on the driven wheels. In the automotive community there are three proposed controller designs for traction control [9]; ABS braking, throttling, and a hybrid of the former two control designs. Sliding mode controllers have been implemented by [10], [9], [6], [8], and [11] to determine the required wheel torque to drive wheel slip to a desired value. For each control design the sliding surface consisted of the error between the desired wheel slip and the actual wheel slip. Boo et al. [9] argued that another method to mitigate traction loss is to control the engine torque through actuation of the throttling valve. Since the

engine torque is coupled to the wheel torque through the drive train, a reduction in engine torque corresponds to a reduction in wheel torque. A PID controller was proposed by Boo et al. [9] to drive the throttling valve to a desired angle. Sunwoo et al. also proposed a sliding mode controller to drive the manifold pressure to a desired value by actuating the throttling valve. The difficulty in using the throttling valve to reduce the engine torque is defining an appropriate engine model. A mean value engine model was used by Boo et al. [9] while Kango et al. [8] utilized a maximum spark advance for best torque model. Implementing their methodology in simulation, Boo et al. [9] improve the stability and acceleration of the vehicle

Unlike automobiles, mobile robots travel at a lower speed and their wheels are often independently driven using DC motors. For mobile robots Ingnemma and Dubowsky [3] proposed a rough terrain optimal controller. Depending on the terrain characteristics, the rough terrain controller either maximized traction force on rough terrain or minimized the power consumption on the motors in benign terrain. In experimentation they compared their rough terrain controller with a velocity controller. In comparing their controllers, they showed their rough terrain controller improved moving over rough terrain by 133%. They argued their rough terrain controller was able to optimize the amount of shear the terrain could bear where as the velocity controller only applied the required torque to satisfy the desired velocity reference. Unlike Ingnemma and Dubowsky [3], Tonizuka and Tai [12] proposed a Backstepping controller capable of tracking a desired reference while mitigating traction loss due to wheel slip. They incorporated a simplified tire model that assumed wheel slip was contained to a linear region. Using this estimate they derived a Backstepping controller that drove the vehicle to a desired reference while

compensating for wheel slip. Their control law, however, was founded on the inverse of the angular velocity. This control law, therefore, was susceptible to an unbounded control input if the angular velocity approached zero. In simulation, their controller was able to produce repeatable results by driving the vehicle to a desired velocity the controller while mitigating traction loss. In their results, however, they did not provide a plot of the angular velocity of the wheel, nor did they discussion the potential of their controller becoming unbounded when the angular velocity approached zero.

Our proposed traction estimation algorithm too requires the uses of a Kalman filter it acquire a best estimate of the wheel slip velocity. Our Kalman filter is unique in that it arrives at a better estimate of the wheel slip velocity by feeding into the Kalman filter an estimate of the wheel torque disturbance. We utilize the estimate of the wheel slip velocity in our traction controller, which is capable of mitigating traction loss while tracking a velocity reference.

2.1. Pacejka's Tire Model

To provide mobile robots the capability of estimating when traction loss occurs, a model describing the interaction between traction and a wheel must be acquired. Pacejka [4] determined an empirical tire model describing the interaction between vehicle dynamics and tire forces. This tire model is known as the Pacejka's Tire Model.

This model utilizes several variables for estimating traction forces. Assuming the only required parameters are the normal force, the terrain characteristics, and the vehicle dynamics, this tire model is reduced to

$$F(t) = f(\lambda(t)), \tag{1}$$

where $F(t)$ denotes the longitudinal friction force and λ is the slip ratio. The slip ratio is defined as

$$\lambda(t) = 1 - \frac{v}{\omega r}, 0 \leq \lambda \leq 1, \tag{2}$$

where v is the linear velocity of a vehicle, ω is the angular velocity of a tire, r is the radius of the tire, and v/r is defined as the relative ground velocity

Figure 2 is an example of implementing(1), which provides an estimate of the friction coefficient, μ, as a function of the slip ratio, λ. In the figure, the horizontal line at $\mu = 0.5$ represents the maximum attainable friction coefficient, and the vertical line at $\lambda = 0.2$ represents the value of wheel slip at the maximum attainable friction coefficient. The friction coefficient was chosen to be the output variable due to its independence from the normal force. Upon inspection of the figure, certain causal relationships can be

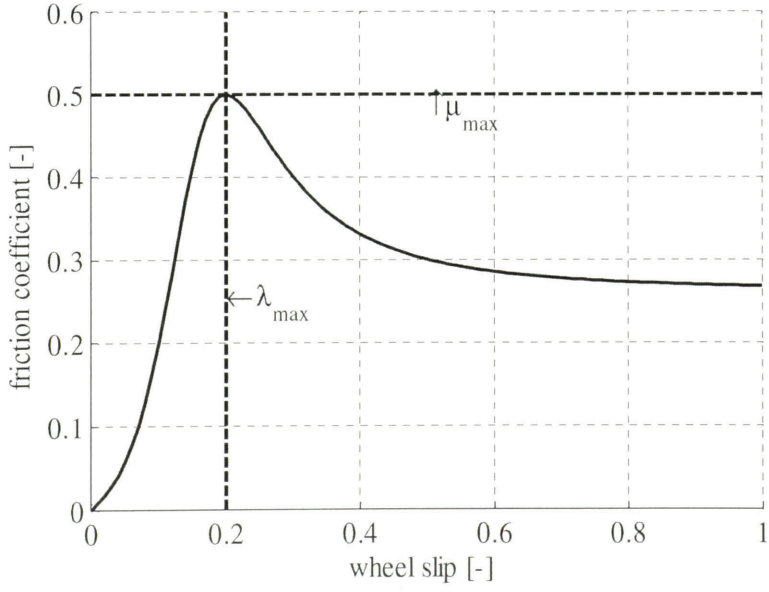

Figure 2: Regions of stability for Pacejka's time model

developed that build the foundation for the proposed traction estimation algorithm.

The first causal relationship is when $\lambda \equiv 0$. At this point the relative ground velocity of the vehicle matches linear velocity. This corresponds to the ideal kinematic constraint of pure rolling without slip. The traction at this point is zero.

One unique characteristic of Pacejka's Tire Model is that the friction coefficient reaches a maximum. Before this maximum is reached the friction coefficient is monotonically increasing with wheel slip, Figure 2. Since the friction coefficient correlates with the longitudinal traction force, the longitudinal traction force available on the surface increases as the wheel slip increases, and, therefore, traction loss is not occurring. Thus, maximizing the available traction on a surface requires that some degree of wheel slip. The shape of the slip curve, however, is unique for every surface. For example, dry asphalt provides more traction that ice. Traction loss, therefore, will occur quicker on ice than on dry asphalt. Terrain characteristics, however, are not the only contributing factor in the shape of the slip curve. The characteristics of a tire also play a role in the shape of the slip curve. Tire pressure, tire wear, tire tread, tire stiffness all contribute to the overall shape of the slip curve. The surface and tire characteristics, therefore, play effect when the peak in the slip curve occurs. Understanding that wheel slip is necessary to maximize traction defines the second causal relationship.

The second causal relationship, therefore, is defined in a region $D \subset R^2$. This region is defined mathematically as $D = \{\mu, \lambda \in R^2 \mid 0 < \mu < \mu_{\max}, 0 < \lambda < \lambda_{\max}\}$. In this region the friction coefficient, μ, and the slip ratio, λ, are monotonically increasing. Since the friction coefficient correlates to the longitudinal traction force, this shows that in region D there is traction available to accelerate a vehicle.

The third causal relationship is defined after the peak of the slip curve, Figure 2. At the peak of the slip curve any further increase in wheel slip results in a decrease in the friction coefficient. The friction coefficient is, therefore, monotonically decreasing with wheel slip. The terrain characteristics, therefore, are not able to sustain the increase in wheel slip. The increase in the wheel slip ratio is a resultant of the wheel speed dominating over the linear velocity of the vehicle. In most instances the linear velocity of the vehicle is being driven to zero due to traction loss while the wheel maintains a constant wheel speed. When the slip ratio equates to the value of one, the system is in pure slip. In pure slip, the angular velocity of the wheel is spinning and the relative ground velocity is zero. Traction loss, therefore, is occurring after the peak in the slip curve and defines the third causal relationship.

The third causal relationship is defined in region $G \subset R^2$. This region is defined mathematically as $G = \{\mu, \lambda \in R^2 \mid \mu_{\max} < \mu \leq \mu_f, \lambda_{\max} < \lambda \leq 1\}$. In this region, μ is monotonically decreasing while λ is monotonically increasing and, consequently, traction loss is occurring.

The peak in the slip curve, therefore, is a critical point of stability in the slip curve. An increase in wheel slip results in traction loss while a decrease in wheel slip results in maintaining traction. To maintain traction, therefore, requires that the wheel slip does not exceed peak in the slip curve. Defining regions of interest in the slip curve enables a heuristic to be defined. This heuristic can be used for traction control.

This heuristic can be derived through inspection of the slip curve. Assuming the friction coefficient, μ, and the slip ratio, λ, are sensible parameters, a heuristic can be derived that will ensure that traction is maintained. Van de Burg et al. [13] showed

traction loss can be estimated by knowing the slope of the slip curve. Through their approach was derived using the Dugoff Tire Model, [14], their approach is valid for Pacejka's Tire Model.

Inspection of the derivative of the Pacejka's' Tire Model enables the ability to estimate traction loss. Knowing the derivatives of μ and λ are monotonically increasing before the peak in the slip curve, the derivative of the slip curve is defined as

$$\frac{dF(t)}{d\lambda(t)} = mg\sin(\theta)\frac{d\mu(t)}{d\lambda(t)} = mg\sin(\theta)\frac{\dot{\mu}(t)}{\dot{\lambda}(t)}, \tag{3}$$

where m is the mass of the vehicle supported by the wheel and $g\sin(\theta)$ is the angular component of gravity. Before the peak in the slip curve, traction is maintained since the derivative of the slip curve is positive. After the peak in the slip curve, however, the derivative of the slip curve is negative, delineating that traction loss is occurring.

$$mg\sin(\theta)\frac{\dot{\mu}(t)}{\dot{\lambda}(t)}, 0 <, \forall \mu, \lambda \in G. \tag{4}$$

By measuring the friction coefficient and the slip ratio, the derivative of the slip curve can be calculated. To maximize traction, the derivative of the slip curve should be contained near the peak of the slip curve. If by causality the derivative is negative, the system should be driven to decrease the wheel speed until the derivative is positive.

There are challenges, however, in estimating the slope of the slip curve. Recall the slip curve is unique for every surface. Variations in the parameters of the wheel also dictate the shape of the slip curve. A bald wheel traveling over asphalt, therefore, will have a different slip curve that a new tire traveling over asphalt. A mobile robot may

encounter packed dirt, loose sand, sand with rocks, and mud, or any other combination of surfaces during its expedition. Estimating the slope of the slip curve for any surface and wheel characteristic, therefore, is an arduous process. There are also major challenges estimating wheel slip.

In determining the traction available on a surface or the derivative of the slip curve requires a good estimate of the wheel slip. For applications where the wheel speed and relative ground speed are high, estimating wheel slip is simple since both parameters are well defined. The wheel slip ration, however, is not well defined for low speed applications where each wheel of a mobile robot is independently actuated. An estimate of wheel slip ratio is ill posed when the angular velocity of the wheel is small. Also a mobile robot accelerating from rest poses a difficult problem for estimating wheel slip. Subtle differences in estimating the relative ground speed and the linear velocity of a vehicle accelerating from rest result in a poor estimate of wheel slip. We propose the wheel slip velocity should be used for low speed application instead of wheel slip.

Though our traction estimation algorithm does not at this time allow for an estimate of the slope of the slip curve, we do propose the wheel slip velocity should be used for estimating the slope of the slip curve for low speed applications. To validate this claim, however, requires an estimate of the traction force, which is the subject of future work. Pacejka's Tire model, however, was an integral part of developing the dynamic equation representing the wheel slip velocity and wheel slip acceleration.

3. TRACTION ESTIMATION FOR A MOBILE ROBOT

3.1. Introduction

In this section we introduce our proposed traction estimation algorithm. Unlike [3] and [15], which use shear forces to estimate traction loss, we propose using an alternate approach. Our traction estimation algorithm models the dynamics of the wheel and the dynamics of the vehicle by using Pacejka's Tire model [4]. By coupling the vehicle dynamics and Pacejka's Tire Model, our traction estimation algorithm model provides an estimate of the wheel slip velocity and wheel slip acceleration through a first order differential equation. The wheel slip velocity and its derivative can be estimated using onboard sensors. Encoders measure wheel odometry while an accelerometer measures the acceleration of the vehicle. To provide a good estimate of the wheel speed we present a modified Kalman Filter that gives a better estimate of encoder data. This Kalman Filter is unique in that is fuses encoder data with an estimate of motor torque disturbances to arrive at a better estimate of the wheel speed. Using this estimate of the wheel speed provides a better estimate of the wheel slip velocity and wheel slip acceleration.

To validate our traction estimation algorithm we conducted tests on carpet and sand. To ensure experiments with repeatable wheel slip we designed an output feedback controller to control wheel speed. Using this control law we provided the ability of tracking a predetermined angular velocity reference. Given this reference our experiments were able to produce repeatable wheel slip. Through our results we show our

traction estimation algorithm provides the ability of estimating traction loss. Using the wheel slip velocity and wheel slip acceleration, a neighborhood can be defined between two instances in time where traction loss is occurring. This neighborhood provides a qualitative estimate of traction loss. By conducting experiments on different surfaces our traction estimation algorithm also provided the ability of estimating traction loss on hard and soft surfaces.

3.2. Overall Traction Estimation Algorithm

Figure 3 represents a block diagram of our proposed traction algorithm for one wheel. This same block diagram can be run in parallel to model our traction algorithm on multiple wheels. The control input, u, from our controller is sent to the plant, which represents the dynamics for the wheel and the vehicle. Our plant produces two outputs. The first is the angular velocity, ω, measured by an optical encoder and the second is the relative ground velocity, v/r, measured by a single axis accelerometer. A better estimate of the angular velocity is achieved using our modified Kalman Filter. Our modified Kalman Filter is comprised of a torque disturbance observer and a Kalman Filter. The wheel slip velocity, α, and the wheel slip acceleration, $\dot{\alpha}$, are estimated using the estimate of the angular velocity, $\hat{\omega}$ and the relative angular velocity, v/r.

3.3. Wheel Slip Velocity and Wheel Slip Acceleration Estimation

As mentioned in our introduction, there are difficulties in estimating the wheel slip and its time derivative. Estimation of wheel slip is difficult for low speeds and its time derivative is unbounded when the wheel speed is constant. Our objective for our proposed traction estimation algorithm is to determine a method to negate an estimate of

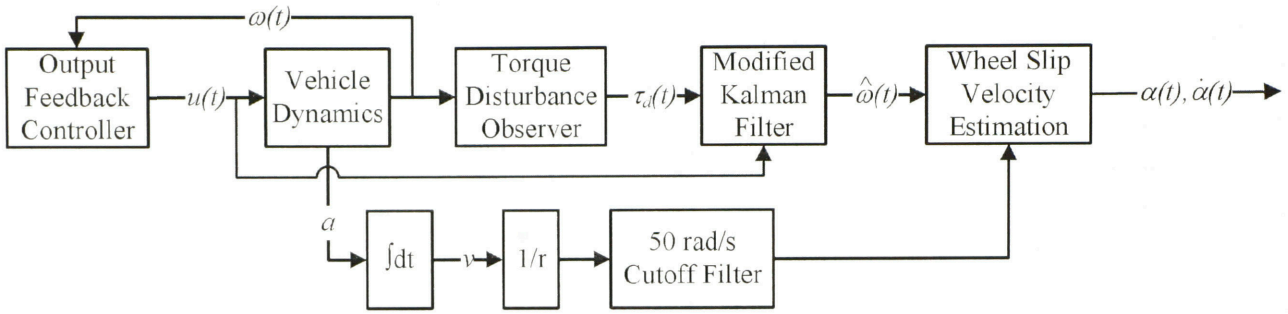

Figure 3: Block diagram representing the process for estimating the wheel slip velocity and wheel slip acceleration

the wheel slip. In deriving our algorithm we introduce a unique parameter denoted as the wheel slip velocity, α, and the wheel slip acceleration, $\dot{\alpha}$. Using the wheel slip velocity and wheel slip acceleration we are able to determine when unstable wheel slip is occurring. We arrive at the definition of the wheel slip velocity by coupling the dynamics of the vehicle and the dynamics of the wheel using Pacejka's Tire Model.

To accomplish this, assume the dynamics of a vehicle is given as

$$\hat{m}\dot{v} + \hat{b}v = F\,, \tag{5}$$

where $\hat{m}$ and $\hat{b}$ are estimates of the mass and damping of the vehicle and F is the forcing on the system modeled by Pacejka's Tire Model. Solving the equation of the wheel slip ratio, (2) , for v and $\dot{v}$ yields

$$\begin{aligned} v &= \omega r(1-\lambda), \\ \dot{v} &= \dot{\omega} r(1-\lambda) + \omega r\dot{\lambda} \end{aligned}. \tag{6}$$

Substituting equation (6) into equation (5) gives

$$\hat{m}\left[\dot{\omega} r(1-\lambda) - \omega r\dot{\lambda}\right] + \hat{b}\left[\omega r(1-\lambda)\right] = F\,. \tag{7}$$

Recognizing the derivative of $\omega\lambda$ appears in equation (7) allows the equation to be rearranged into the form,

$$\dot{\omega}\lambda + \omega\dot{\lambda} = -\frac{\hat{b}}{\hat{m}}\omega\lambda + \dot{\omega} + \frac{\hat{b}}{\hat{m}}\omega - \frac{F}{\hat{m}r}\,. \tag{8}$$

Equation (8) can simplified using the change of variables,

$$\alpha = \omega\lambda, \dot{\alpha} = \dot{\omega}\lambda + \omega\dot{\lambda}, \tag{9}$$

where α is the wheel slip velocity and $\dot{\alpha}$ is the wheel slip acceleration. By substituting the wheel slip velocity and the wheel sip acceleration into equation (8) results in a general linear differential equation. This differential equation forms the foundation of our traction estimation algorithm by establishing the dynamic relationship between the wheel slip velocity and the wheel slip acceleration. Substitution equation (9) into equation (8), allows this equation to take the form of

$$\dot{\alpha} = -\frac{\hat{b}}{\hat{m}}\alpha + \left(\dot{\omega} + \frac{\hat{b}}{\hat{m}}\omega\right) - \frac{F}{\hat{m}r}. \tag{10}$$

The difficulty in equation (10) is determining the vehicle time constant, $\frac{\hat{b}}{\hat{m}}$ since an estimate of the vehicle's damping is unknown. An estimate of the vehicle time constant, however, can be replaced through inspection of the dynamics of a wheel. Assuming the dynamics of a wheel follow the general form,

$$\begin{aligned} &\tau = \hat{J}\dot{\omega} + \hat{B}\omega, \\ &\therefore \frac{\tau}{\hat{J}} = \dot{\omega} + \frac{\hat{B}}{\hat{J}}\omega = \dot{\omega} + \frac{\hat{b}}{\hat{m}}\omega, \end{aligned} \tag{11}$$

where $\hat{B}$ is an estimate of rotational damping and $\hat{J}$ is an estimate of the rotational moment of inertial. The major assumption in equation (11) is that the time constant of the motor $\frac{\hat{B}}{\hat{J}}$ is equal to the time constant of the vehicle, $\frac{\hat{b}}{\hat{m}}$. By replacing the time constant of

the vehicle with the time constant of the motor transforms equation (10) into estimated parameters of the wheel. The parameter, $\frac{F}{\hat{m}r}$, can also be transformed by assuming,

$$\frac{F}{\hat{m}r} = \left(\frac{r}{r}\right)\frac{F}{\hat{m}r} = \frac{F}{\hat{m}r^2} = 2\frac{Fr}{\hat{J}}, \tag{12}$$

Substituting these assumptions, Equations (11)and(12), into equation (10) results in a first order differential equation that estimates the wheel slip velocity and wheel slip acceleration,

$$\dot{\alpha} = -\frac{\hat{B}}{\hat{J}}\alpha + \frac{1}{\hat{J}}(\tau - Fr). \tag{13}$$

Through analysis of equation (13) the dynamic relationship between the wheel slip velocity and the wheel slip acceleration is established. Assuming the wheel is traveling over an ideal surface, the wheel torque, τ, equates to the traction torque, Fr. The wheel slip velocity, therefore, will asymptotically converge to zero. If traction loss occurs the wheel torque does not equate to the traction torque. Assuming the difference between the wheel torque and the traction torque is constant for all time the wheel slip velocity will have a first order response and will asymptotically converge to steady state. The wheel slip velocity, therefore, is asymptotically stable.

Though the dynamic equation representing the wheel slip velocity is stable, the driving assumption in the stability this equation is estimation of both the wheel torque and the traction torque. The wheel torque can be estimated using the back EMF constant of a DC motor, the current running through the DC motor, and the gear ratio between the motor and the wheel. An estimate of the traction torque, however, is difficult to

determine due to the nonlinear behavior of Pacejka's Tire Model. Assuming the vehicle is constrained to travel over a homogeneous surface Pacejka's Tire Model can be empirically estimated. Providing an estimate of the traction force on homogenous and expanding it to heterogeneous terrains was not investigated. Validating the use of using the wheel slip velocity for low speed application over the traditional use of wheel slip was considered a higher priority. Providing an algorithm capable of estimating the traction force, however, does provide the ability of using equation (13) as an observer for the wheel slip velocity. Though equation (13) relies upon the use of the traction force to arrive at an estimate of the wheel slip velocity, it will be shown that the wheel slip velocity can be estimated using sensory data.

By expanding the definition of the wheel slip velocity from (9) is can be shown that estimates of the wheel slip velocity and wheel slip acceleration can me measured using onboard sensors. By substituting the equation for the wheel slip ratio into equation (9) yields

$$\alpha = \omega - \frac{v}{r}, \dot{\alpha} = \dot{\omega} - \frac{\dot{v}}{r}. \tag{14}$$

The wheel slip velocity therefore can be estimated by measuring the angular velocity of the wheel and the linear velocity of the vehicle. Using equation (14) reduces the complexity of estimating the traction torque in equation (13).

In linear and nonlinear feedback control the error state is used to drive a system to its desired reference. Recall in the background that several Authors used the error of wheel slip to mitigate traction loss. The error of wheel slip, therefore, is an error state between two ratios. Equation (14) defines the wheel slip velocity and wheel slip acceleration as

the error between the dynamics of the wheel and the dynamics of the vehicle. By definition the wheel slip velocity and wheel slip acceleration are pure error states. In other words the error states do not require any complex mathematical operations besides addition and subtraction. Wheel slip velocity and the wheel slip acceleration, therefore, are not prone to division by zero like wheel slip. The error of wheel slip, however, is not a pure error state. Thus, the wheel slip velocity and acceleration provides an ideal error state for feedback control, which can be used for any traction control system for low speed applications.

By modifying the dynamics of the vehicle using Pacejka's Tire Model (5) , we removed the necessity of determining the wheel slip ratio by introducing the wheel slip velocity. Though the dynamic response of the wheel slip velocity is modeled after a first order system, this model requires an estimate of the wheel torque and the traction torque. Recognizing the difficulty in measuring the traction torque using the Pacejka's Tire Model, it was shown that the wheel slip velocity and wheel slip acceleration could be estimated using the angular velocity the wheel and the linear velocity of the vehicle. Though the derivation of the wheel slip velocity included only a single wheel, this method can be coupled to a multiaxle vehicle. Measurement of the wheel slip velocity is possible by independently sensing the angular velocity of each wheel and measuring the linear velocity contribution of each wheel. Determining the linear velocity contribution for each wheel requires knowledge of the traction force. An estimate of the traction force, therefore, is not only critical in using equation (13) as an observer for the wheel slip velocity but is important for using the wheel slip velocity for a multiaxle mobile robot. Gaining an estimate of the traction torque, therefore, is the next evolutionary step

required to advance the understanding of using the wheel slip velocity for traction control in low speed applications.

3.4. Kalman Filter Design

3.4.1. General Kalman Filter Design

To achieve a good estimate of traction loss requires a good estimate of the wheel slip velocity and wheel slip acceleration. Both these parameters can be measured using onboard sensors, optical encoders for wheel odometry and accelerometers for linear velocity. Both forms of measurement, however, are prone to error when computing derivatives or integrals. Computing the derivative is sensitive to sensory noise whereas computing the integral is susceptible to sensory drift. The wheel slip acceleration, therefore, is prone to error from computing the derivative of the angular acceleration, and the wheel slip velocity is prone to error from integrating linear acceleration. Our objective is to determine a better estimate of the wheel slip acceleration we propose implementing a Kalman Filter.

The general state equation representing the dynamics of a wheel takes the following form with unknown process noise, w, and output noise, v;

$$\begin{aligned} \dot{x} &= \mathbf{A}x + \mathbf{B}u + \mathbf{G}w, \\ y &= \mathbf{C}x + v, \\ \mathbf{A} &= -\frac{\hat{B}}{\hat{J}}, \mathbf{B} = \frac{K_t}{R_m \hat{J}}, \mathbf{C} = 1, \mathbf{G} = 1, \end{aligned} \tag{15}$$

where x represents the angular velocity of a wheel, u is the motor voltage input, and y is the output of our state model provided through encoder data. $\hat{B}$ and $\hat{J}$ are the estimates

of the mechanical damping and the inertia of the wheel. The electrical components of the armature of the DC motor, K_t and R_m, are the torque constant of the motor and the resistance of the armature. The signal w is an unknown process noise acting on the plant from the voltage input. The signal v is unknown measurement noise from the encoder.

We desire to design a Kalman Filter to provide a better estimate of the angular velocity of the wheel. Assume the observer to estimate the angular velocity takes the form

$$\dot{\hat{x}} = \mathbf{A}\hat{x} + \mathbf{B}u + \mathbf{L}(y - \hat{y}), \tag{16}$$

where $\mathbf{L}$ is the observer gain to provide an optimal estimate of the angular velocity in the presence of the process noise, w, and the output noise, v. To determine the appropriate observer gain, the error covariance, $\mathbf{P}$, must be solved using the algebraic Riccati equation

$$\mathbf{AP} + \mathbf{PA}^T + \mathbf{GQG}^T - \mathbf{PCR}^{-1}\mathbf{CP} = 0, \tag{17}$$

where $\mathbf{R}$ is the covariance of the output noise, and $\mathbf{Q} = \mathbf{C}^T\mathbf{C}$. Solving for the error covariance, $\mathbf{P}$, provides the ability to determine the optimal observer gain, $\mathbf{L}$ where

$$\mathbf{L} = \mathbf{PC}^T\mathbf{R}^{-1}. \tag{18}$$

This Kalman Filter design uses the ideal system model of a DC motor to acquire a better estimate of the angular velocity. The ideal system model of a DC motor, however, does not account for disturbances acting on the system. Unknown disturbances acting on the system will cause a larger deviation between the actual angular velocity and the

estimate of the angular velocity. Larger deviations in the measured versus estimated angular velocity require the optimal observer gain to weigh a higher confidence in the measured data. Placing higher confidence in the measured data results in a poor estimate of the angular velocity since the output noise is not rejected by the Kalman Filter. We propose a modified Kalman Filter that uses an estimate of wheel disturbances to provide a better estimate of angular velocity.

3.4.2. Modified Kalman Filter Design

Our modified Kalman Filter utilizes an estimate of the disturbance torque, τ_d, applied to the wheel in order arrive at an accurate estimate of the angular velocity of the motors. To estimate the disturbances torque we propose a wheel disturbance torque observer. Our wheel disturbance torque observer obtains an estimated the disturbance torque by comparing the predicted response of the motor to the sensed response of the motor. To derive our wheel disturbance torque observer, assume the ideal motor model takes the form of

$$\dot{\omega} = -\frac{\hat{B}}{\hat{J}}\hat{\omega} + \frac{K_t}{R_m \hat{J}}u \,. \tag{19}$$

The angular velocity, $\hat{\omega}$, and the angular acceleration, $\dot{\hat{\omega}}$, are derived as estimates since the motor model is ideal and does not represent the actual system. Let the actual response of the motor be represented as

$$\dot{\omega} = -\frac{\hat{B}}{\hat{J}}\omega + \frac{K_t}{R_m \hat{J}}u + \tau_D \,, \tag{20}$$

where τ_D is an unknown disturbance torque. Our objective is to estimate the unknown disturbance. To estimate the unknown disturbance torque subtract equation (19) from equation (20) which yields,

$$\begin{aligned} \tau_D &= \dot{e} + \frac{\hat{B}}{\hat{J}} e, \\ e &= \omega - \hat{\omega}, \dot{e} = \dot{\omega} - \dot{\hat{\omega}}, \end{aligned} \tag{21}$$

Equation (21) represents our proposed disturbance torque observer. By coupling the estimate of the disturbance torque into our proposed Kalman Filter provides a more complete model of the dynamics of the wheel, resulting in a better estimate of the angular velocity.

Coupling the estimate of the disturbance torque into the Kalman Filter design yields

$$\begin{aligned} \dot{\hat{x}} &= \mathbf{A}\hat{x} + \mathbf{B}u + \mathbf{L}\left(y - \hat{y}\right) + \tau_D, \\ \mathbf{A} &= -\frac{\hat{B}}{\hat{J}}, \mathbf{B} = \frac{K_t}{R_m \hat{J}}, \end{aligned} \tag{22}$$

where $\mathbf{L}$ is the optimal Kalman Filter Observer gain. This modified Kalman Filter is the design we propose to accurately estimate the wheel speed. To determine the optimal observer gain for this modified Kalman Filter Design we experimentally modified $\mathbf{L}$ until a good estimate of the angular velocity was achieved.

Not only does estimating the torque disturbance, Fig. 3, for each wheel provide a better estimate of the angular velocity, but the disturbance torque can also be used to derive an estimate of the traction forces. Deriving an observer for traction forces provides the ability of estimating the individual linear velocity contribution of each wheel to the motion of the vehicle. Knowing the individual linear velocity contribution of the wheels

provides a better estimate of the wheel slip velocity for each wheel. Deriving an observer to estimate the traction forces from the estimate of the torque disturbance is a subject for future research.

3.5. Output Feedback Control

To assure our traction estimation algorithm provides the ability of measuring the qualitative behavior of traction loss, the full spectrum of the slip curve must be explored. The wheel slip, therefore, has to range from zero to one, which implies that the wheel slip velocity has to range from zero to $\alpha = \omega$. To accurately control the angular velocity of the wheel we propose a control law that tracks a desired reference angular velocity. Our control law uses linearization to drive the angular velocity to the desired reference. The placement of this controller in our traction control algorithm is noted in Figure 3.

Our objective is to design an output feedback controller capable of following a desired angular reference trajectory, θ_r . It is assumed the angular reference trajectory is differentiable. To derive our proposes control law let the ideal motor model described in equation (19) take the form

$$\ddot{\theta} = -\frac{\hat{B}}{\hat{J}}\dot{\theta} + \frac{K_t}{R_m \hat{J}}u\,, \tag{23}$$

where θ is the angle of the wheel. For the wheel to follow the desired angular reference trajectory a certain voltage must be applied across the motor. Assuming the motor to be at steady state, the required voltage can be estimated by

$$u_r = \frac{\hat{B}R_m}{K_t}\dot{\theta}_r\,, \tag{24}$$

where u_r is the required voltage input. Taking the angular reference trajectory and the required voltage input the error states for equation (23) can be derived using

$$\begin{aligned} x_1 &= \theta - \theta_r, \\ x_2 &= \dot{\theta} - \dot{\theta}_r, \\ v &= u - u_r \end{aligned} \tag{25}$$

where x_1 and x_2 are the error states and v is the control input. Substituting the error states into equation (23) transforms the dynamics of the motor into state form

$$\begin{aligned} \dot{x}_1 &= x_2, \\ \dot{x}_2 &= -\frac{\hat{B}}{\hat{J}}\left(x_2 + \dot{\theta}_r\right) + \frac{K_t}{R_m \hat{J}} v, \\ y &= x_1, \end{aligned} \tag{26}$$

where y sensed output of the system. Regulation of the state equation in equation (26) can be achieved by using an output feedback controller. Let the output feed back controller take the following form,

$$v = -\mathbf{K}y, . \tag{27}$$

Substituting the control law into the transformed state model yields

$$\begin{aligned} \dot{x} &= \left(\mathbf{A} - \mathbf{BKC}\right) x, \\ \mathbf{A} &= \begin{bmatrix} 0 & 1 \\ 0 & -\frac{\hat{B}}{\hat{J}} \end{bmatrix}, \mathbf{B} = \begin{bmatrix} 0 \\ \frac{K_t}{R_m \hat{J}} \end{bmatrix}, \end{aligned} \tag{28}$$

where K is designed to make equation (28) stable. Stability is guaranteed if all the real components of the Eigenvectors in $(\mathbf{A} - \mathbf{BKC})$ are negative. Combining equation (25)

with our proposed output feedback controller in equation (27) generates the voltage input that will drive the motor to the desired angular reference trajectory,

$$u = u_r - \mathbf{K}y \,. \tag{29}$$

The benefit of this controller is that it utilizes the reference voltage to assist in driving the system to the desired angular reference trajectory. If there is a tracking error due to an unknown disturbance, the control gain K modifies the control input to drive the system to the desired angular reference trajectory.

3.6. Experimental Setup

3.6.1. Methods and Procedures

To validate our traction estimation, algorithm tests were performed on a single axle mobile robot. Figure 4 provides visual description of the experimental setup. The experimental vehicle consisted of a single axle mobile robot powered by two geared DC motors. Control of the robot was achieved using a tether via dSpace™ 1103 DSP, and power was provided externally. To estimate the wheel speed and the wheel odometry was measured using an optical encoder, Table 1. A single axis accelerometer was mounted to the front of the vehicle with the sensing axis pointed in the direction of motion. Power was provided to the accelerometer by a 7.2v RC battery coupled to a 5v regulator. To stabilize the vehicle a training wheel was mounted to the axle. A linear potentiometer was attached to the back of the training wheel. Power was provided to the linear potentiometer using a 12VDC Power Supply. The signal from the potentiometer was fed

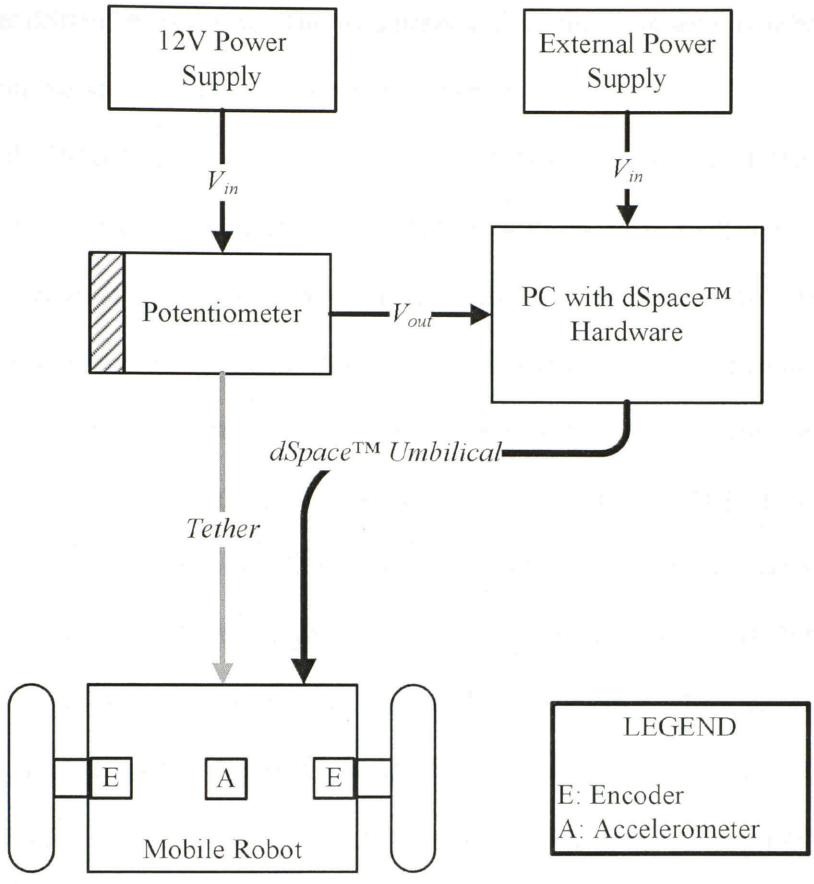

Figure 4: Experimental setup

Table 1: List of sensors used in the design of experiments for estimation of the wheel slip velocity

Sensors	Model Number	Manufacturer
Miniature Position Transducer	160-1285-C8SS	SpaceAge Control
MEMS Capacitive Accelerometers	MS7000	Colibrys
Optical Encoder	E2-1024-250	US Digital

back to the dSpace™ hardware. The resolution and accuracy as well as other technical details about the sensors can be found in the Appendix.

With the retarding force acting on the robot, the linear travel of the robot was dependent on surface conditions. The surface conditions were picked to maintain a maximum traction force less than the maximum tether force. Allowing this relationship to hold provided an experiment that forced pure slip on the wheels of the mobile robot. The sampling rate for the experiments was conducted at 100 Hz to limit sensor noise from the encoder/accelerometer and to reduce chatter from the controller. With this frequency, however, the sensor noise still had to be filtered to provide an accurate measurement of traction loss. Smoothing of the response of the angular velocity of the wheels through the encoders was provided by our proposed modified Kalman Filter. The accelerometer data were also filtered with a cutoff frequency of 50rad/s. Using this cut off frequency smoothed out the output from the accelerometer and did not introduce a significant delay due to phase. The output of the Kalman Filter was fused with the filtered data from the accelerometer to calculate the wheel slip velocity and wheel slip acceleration.

To ensure repeatable wheel slip, our proposed output linear feedback integral controller was designed drive the angular velocity of the wheel to a desired angular reference trajectory. This controller provided repeatable wheel slip in the presence of the variable tether force given the prescribed trajectory. With a working controller, the robot was connected to the tether and tests were performed on carpet and sand with a depth of 1cm. Results for the tests were compiled offline.

3.6.2. Power Amplifier Calibration

The power amplifier for the mobile robot was calibrated to validate that the voltage applied to each wheel equated to the commanded voltage generated using our proposed output feedback controller.Tuning the power amplifier was accomplished by supplying a desired voltage to each wheel. The voltage was then measured on each motor using a multimeter. If the actual voltage did not equate to the desired voltage the power amplifier gain for the motor was adjusted using a set screw until the error was within half a volt.

3.6.3. Linear Potentiometer Calibration

The experimental setup to calibrate the linear potentiometer consisted of a millimeter, a power supply, a linear potentiometer, a ruler, and a set of weights, Figure 5. The purpose of the calibration was to determine the correlation between the output voltage of the linear potentiometer and displacement, Δx. Applying known weights to linear potentiometer also provided a correlation between the output voltage of the linear potentiometer and the applied force.

Each weight was calibrated using a digital scale. The weight was carefully attached to the tether on the linear potentiometer in order to reduce the jerk applied to the sensor. With the weight connected to the linear potentiometer, the weight was slowly lowered until a steady state displacement was reached. The output voltage of the linear potentiometer was recorded from the digital multimeter and the displacement was measured using a meter stick. After the measurements were recorded the weight was removed and the process was continued until all combinations of weights were used.

Using the results from this experimental setup, the conversion from volts DC to distance for the linear displacement was found to be 35mm/V, Figure 6., while the force

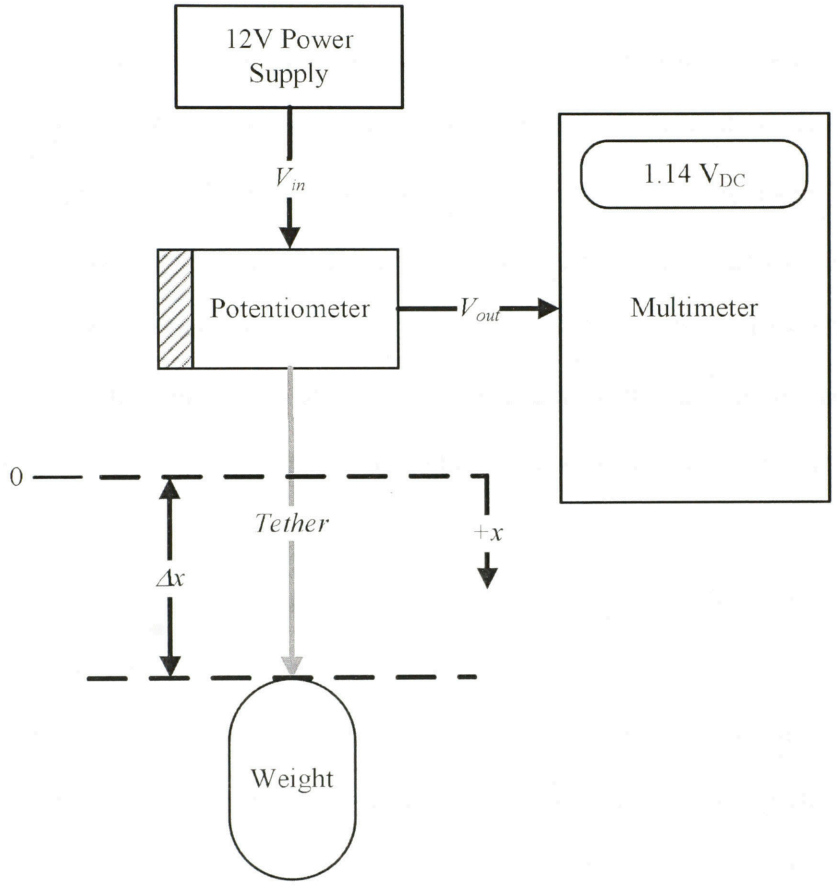

Figure 5: Experimental setup for calibrating the linear potentiometer

profile was parabolic, Figure 7. Using least squares regression the coefficients for the curve were estimated to determine the force applied to the linear potentiometer.

3.6.4. Accelerometer Sensitivity and Calibration

While calibrating the accelerometer in static testing, it was found that the bias offset of the accelerometer was being amplified by vehicle vibrations. These vibrations emanated from the DC motors that actuated the wheels. The vibrations from the DC motors propagated through the axle where the accelerometer was mounted. Since the housing or the accelerometer was fastened to the axle, the axle vibrations introduced base excitation to the accelerometer. From inspection it was noticed that the sensed acceleration due to base excitation was much larger than the sensed acceleration associated. A vibration isolator, therefore, had to be incorporated into the accelerometer hardware.

To minimize the effects of the axle vibrations, a mechanical spring damper had to be inserted between the axle and the accelerometer, Figure 8. This was accomplished by drilling through holes into the accelerometer mounting frame that was larger than the mounting crews of the accelerometer. Foam was stuffed between the mounting screws and the through holes. The foam was also used to separate the accelerometer from the mounting frame and the mounting frame from the axle. This resulted in creating a mechanical damper that reduced the high frequency noise and provided an accurate measurement of the linear acceleration. Since the foam sufficiently reduced the high frequency noise, no other materials were tested. Calibration of the accelerometer was performed online. For each run the mobile robot would remain stationary for one second. The first half a second was used to compute the bias output of the accelerometer, which

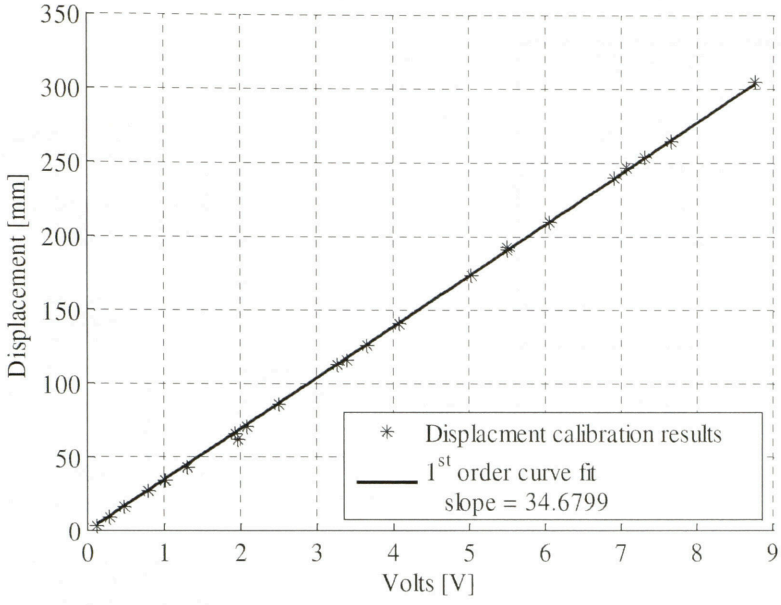

Figure 6: Linear potentiometer displacement profile versus Volts

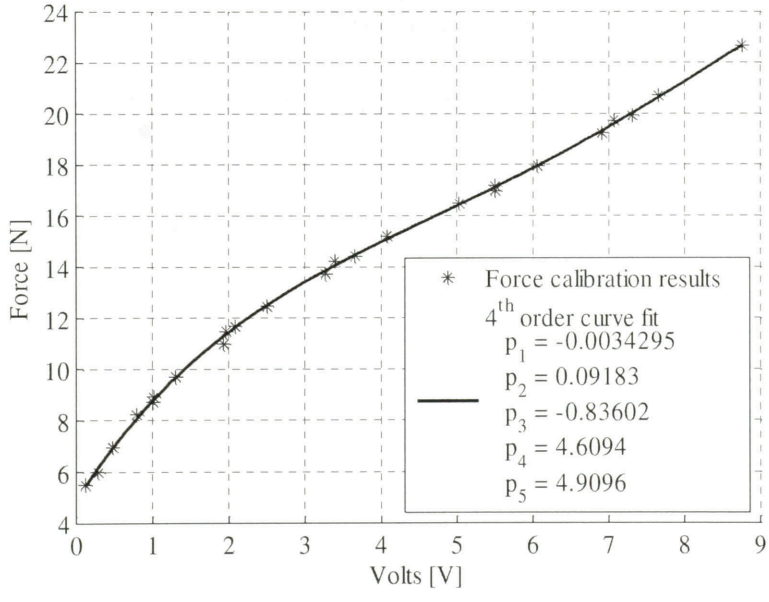

Figure 7: Linear potentiometer force profile versus Volts

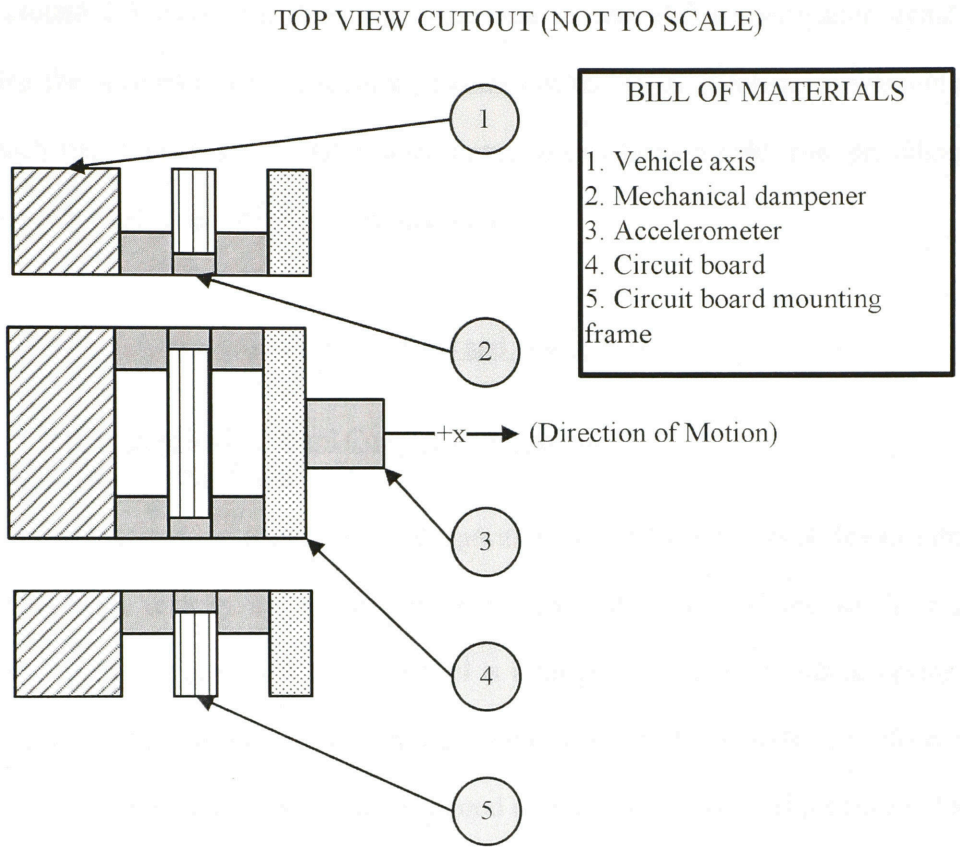

Figure 8: Low pass mechanical damper assembly

was around 2.5 volts. This bias was then used to zero the accelerometer signal. By zeroing the accelerometer, an accurate estimate of the linear acceleration was obtained for each run. Calibration of the accelerometer in this fashion held true, providing the mobile robot did rotate about its principle axis.

3.7. Results and Discussion

3.7.1. Output Feedback Control Coupled to Proposed Modified Kalman Filter

The efficacy of our traction control algorithm is founded upon its ability to estimate the wheel slip velocity and wheel slip acceleration. As discussed previously, a good estimate of the angular speed of the wheel is a progressive step towards achieving that goal. The modified Kalman Filter and the Output Feed Back controller, therefore, were developed as integral tools to facilitate a good estimate of the wheel slip velocity. Figure 7 displays the effectiveness of the proposed modified Kalman Filter and Output Feedback controller.

Our modified Kalman Filter design, utilizing an estimate of the wheel disturbance, provided a better estimate for the angular velocity. By placing full confidence in the encoder signal an accurate representation was produced for the angular velocity of the wheel, Figure 9, 10. The encoder signal, however, was noisy due to the sampling rate of the experiment, the low velocity of the robot, and the encoder resolution. This noisy signal does not allow for a good estimate of the angular velocity of the wheel, and therefore, does not allow for a good estimate of the wheel slip acceleration. By generating an estimate of the disturbance torque, the estimate of the angular velocity of the wheel as smoothed, Figure 11. Using an observer gain of $\mathbf{L}=0.1$ provided an accurate estimate the

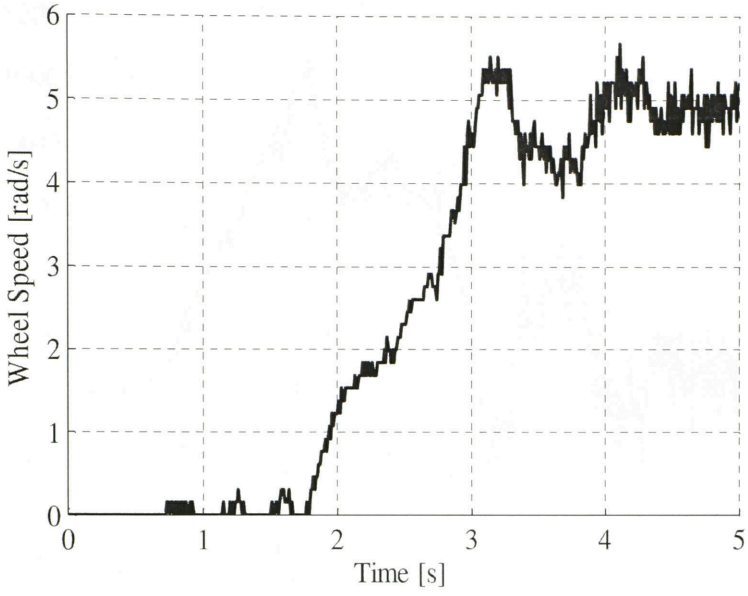

Figure 9: Unfiltered dynamic response of a wheel measured from the wheel encoder

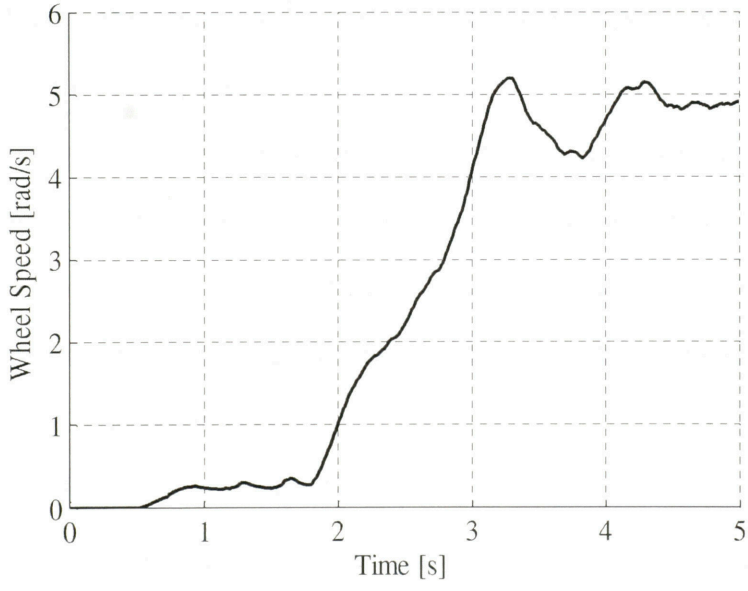

Figure 10: Filtered dynamic response of a wheel implementing the modified Kalman filter

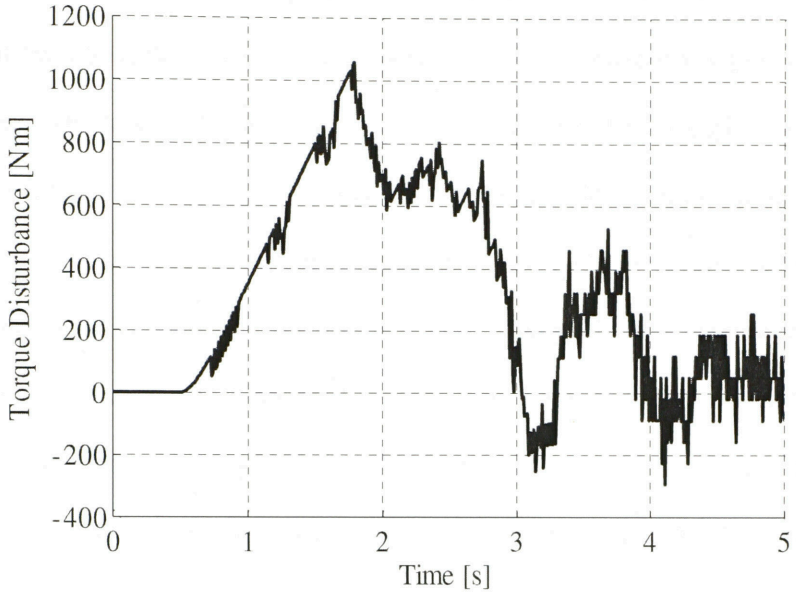

Figure 11: Estimate of the torque disturbance

angular velocity of the wheel. The gain for the modified Kalman Filter was tuned using experimental data. This value for the gain provided an appropriate balance among the confidence of the motor model, the sensed angular velocity, and the estimated disturbance torque. Smoothing out the estimate of the angular velocity provides a better estimate of the wheel slip velocity and the wheel acceleration. If time permitted it would have been beneficial to tune the Kalman Filter Gains as a function of vehicle speed in order to acquire a better estimate of the wheel speed when the magnitude of the wheel speed is small, i.e. less than 0.5 rad/s.

The gains K for the Output Feedback Controller were determined through experimentation. With K=2 the controller was able to effectively drive the system to a desired steady state value of 5 rad/s. As can be seen from Figure 10, the angular velocity oscillates around the desired angular velocity. There was also noticeable lag in the initial response of the angular velocity of the wheel. The lag in the vehicle's response was a

result of the tether force pulling against the vehicle's desired direction of motion. The design of the controller, however, was to drive two independently actuated wheels at the same rate which would result in the vehicle traveling a straight course. Through observation the control gains adequately drove the mobile robot in the desired direction. If time permitted, the control gains could have utilized the control technique of gain scheduling to reject the tether disturbance more adequately, but validating the design of the traction control algorithm took precedence over tuning the control gains. By designing the Output Feedback Controller the vehicle was able to drive a straight course, which resulted in repeatable experiments to validate our proposed traction estimation algorithm.

3.7.2. Qualitative Traction Loss Estimation using the Wheel Slip Velocity

The wheel slip velocity and wheel slip acceleration were estimated using equation (14). Implementing our traction estimation technique, we can determine a neighborhood, *N*, where traction loss is occurring. Figure 12-16 display comparable results for tests conducted on carpet. Each figure contains two vertical lines, which are placed at specific instances in time. These vertical lines define the limits in time, t_1 and t_2, of a neighborhood N where $N = \{t, f(t) \in R^2 \mid t_1 \le t \le t_2\}$. Figure 12 displays the wheel speed, ω, and the relative ground angular velocity, *v*/r, compared to the desired angular velocity reference. Figure 13 displays the results for wheel slip velocity, and Figure 14 displays the wheel slip acceleration. Figure 15, 16 display the displacement and tether force, respectively. The neighborhood, *N*, can be defined on both carpet and sand to estimate when traction

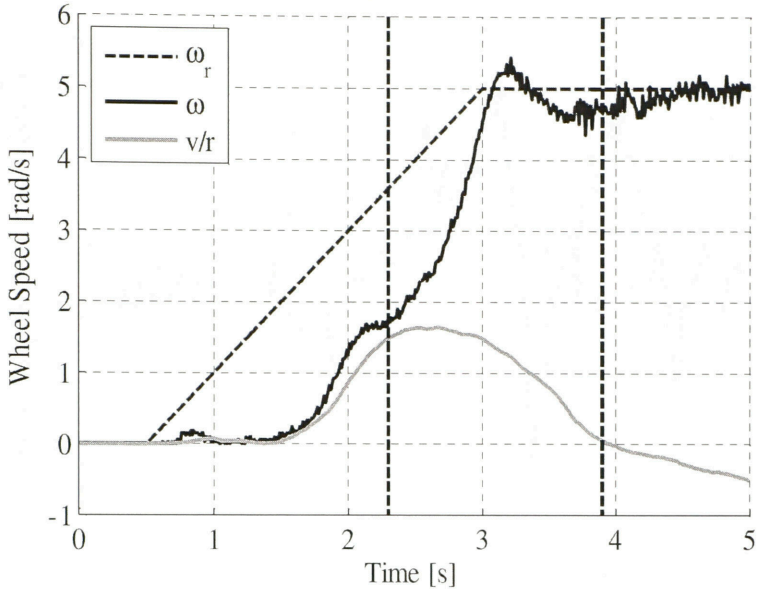

Figure 12: Comparable estimate of the wheel speed and estimate of the relative ground velocity compared to the desired wheel speed reference for experiments conducted on carpet

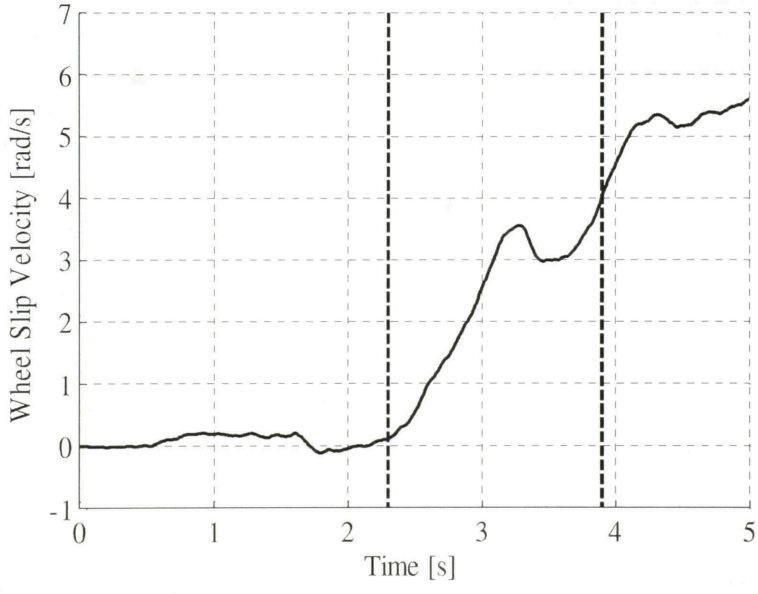

Figure 13: Comparable estimate of the wheel slip velocity for experiments conducted on carpet

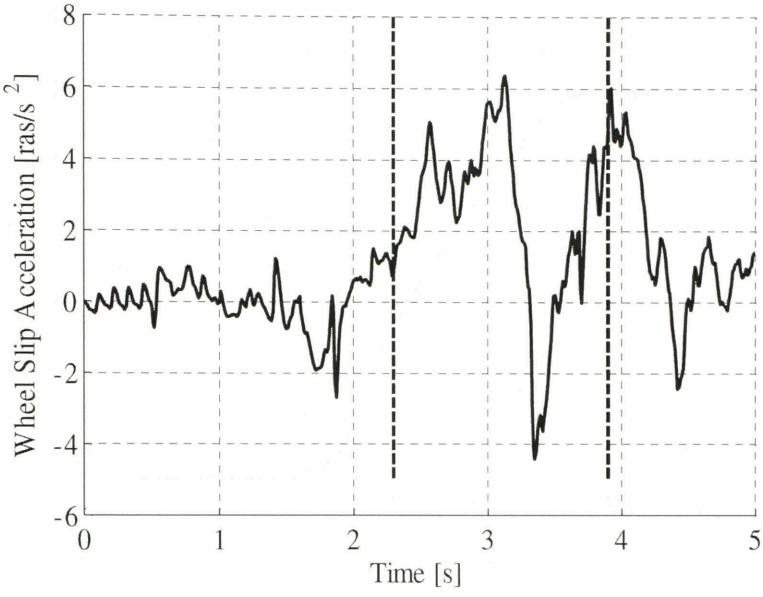

Figure 14: Comparable estimate of the wheel slip acceleration for experiments conducted on carpet

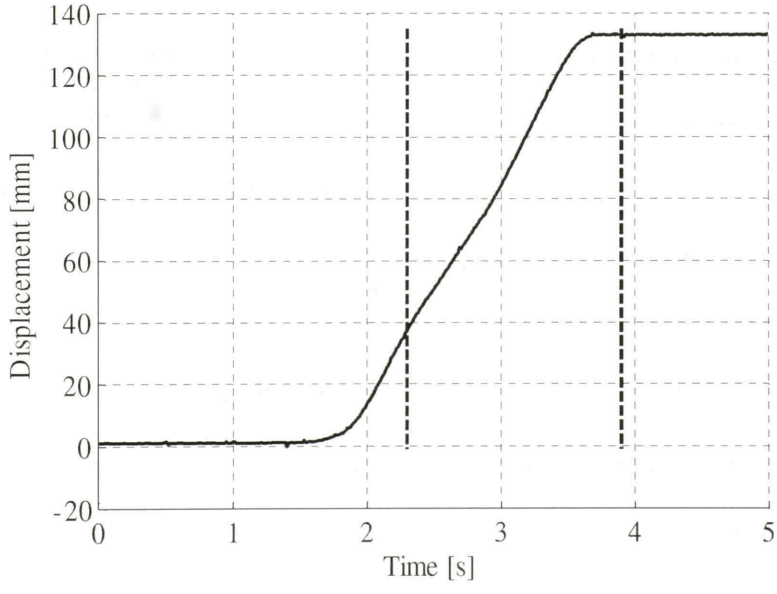

Figure 15: Comparable displacement of the linear potentiometer for experiments conducted on carpet

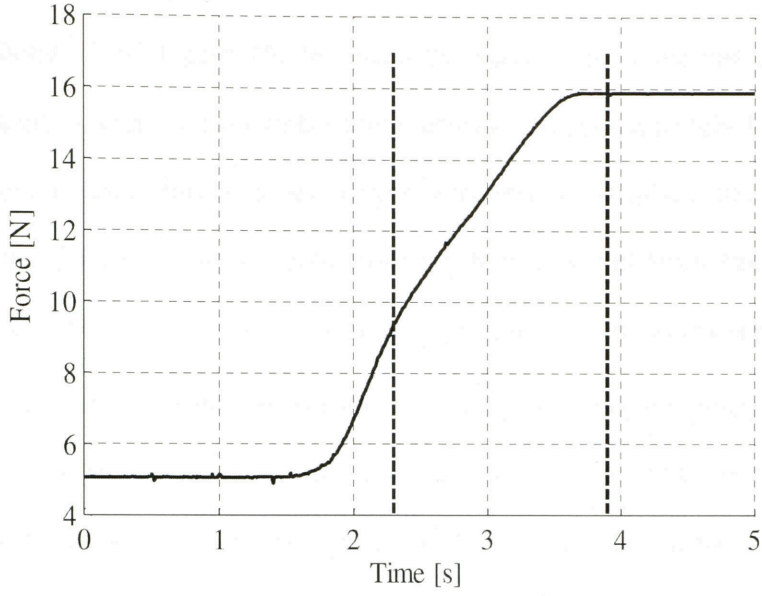

Figure 16: Comparable force on the linear potentiometer for experiments conducted on carpet

loss is occurring. Justification of our algorithm will be contained to the results on carpet since these results typify the performance of our traction estimation algorithm. After proving the validity of our traction estimation algorithm on carpet, the results from our experiments on sand will be discussed.

As can be seen from Figure 12, the two vertical lines define a neighborhood N between 2.3 and 3.9s. Before 2.3s there is no depreciable change between the angular velocity of the wheel, ω, and the relative angular velocity, v/r. The difference between the angular velocity and the relative ground velocity is represented by wheel slip velocity, Figure 13. The wheel slip velocity before 2.3s is below 1rad/s and the time average of the wheel slip acceleration is approximately zero, Figure 14. Before 2.3s traction loss is not occurring since the wheel slip velocity and the wheel slip acceleration are small.

Inspection of the displacement and the tether force also shows that traction loss is not occurring before 2.3s, Figure 15, 16. From the initial start of the test up to 2.3s, the vehicle displaced 60mm ant the tether force increased to approximately 11N. Up to 2.3s the available traction force on the carpet was able to displace the vehicle while compensating for the retarding force from the tether. Recall from Pacejka's traction curve, in the stable region of the curve, $\lambda < \lambda_{max}$, an increase in wheel slip corresponded to an increase in traction force. Wheel slip, therefore, has to occur to instigate an increase in traction force. Before 2.3s the wheel slip increased to approximately 0.75 rad/s. The increase in the wheel slip velocity corresponded to an increase in the tether force. An increase in the wheel slip velocity, therefore, is required for an increase in traction force. Recall when derivative of Pacejka's slip curve is positive, i.e., an increase in wheel slip corresponds to an increase in traction force, traction loss is not occurring. An increase in the wheel slip velocity and an increase in the tether force, therefore, demonstrate traction loss is not occurring.

In the neighborhood *N*, however, traction loss is occurring. In this neighborhood, the tracking controller is attempting to drive the response of the wheel to the desired angular velocity. As the response of the angular velocity is ramping up, the response of the relative angular velocity, however, does not coincide, Figure 12. In this neighborhood the response of the relative angular velocity reaches a maximum at approximately 2.8s and drops to zero at approximately 3.9s. At 2.8s the traction available on the surface is not sufficient to compensate for the increase in the tether force, which results in an increase in the wheel slip velocity.

In the neighborhood, N, the wheel slip velocity has dramatically increased, Figure 13. Since there is a change in the wheel slip velocity, this change is represented by the wheel slip acceleration, Figure 14. In this neighborhood, the wheel slip acceleration forms a positive parabolic curve. This is expected because there is a positive change in angular velocity while there is a negative change in the relative ground velocity. This significant change in the wheel slip acceleration demonstrates that traction loss is occurring in the neighborhood *N*.

Once again, inspection of the displacement and the force show that in the neighborhood, *N*, traction loss is occurring. Between 2.3s and 3.9s the vehicle displaced from 60m to a steady state displacement of 120cm. The tether force too has increased from 11N to a steady state force of 16N, respectively. Recall from Pacejka's Tire Model after the wheel slip has reached its maximum, $\lambda > \lambda_{max}$, an increase in wheel slip corresponds to a decrease in traction force. Traction loss is therefore occurring. Between 2.3s and 3.9s the wheel slip velocity has increased while the tether force has reached a steady state. The available traction on the carpet is not able to compensate for the increase in the tether force. Traction loss, therefore, is occurring in the defined neighborhood since the displacement and the tether force has reached steady state and the wheel slip velocity is increasing.

At 3.9s, the tracking controller has driven the angular velocity to the desired steady state velocity of 5rad/s. The relative angular velocity, however, at this time is zero. The system, therefore, is in pure slip. Since the angular velocity and the relative ground velocity are at steady state, the wheel slip acceleration is approximately zero. An important note is that the value of the wheel slip acceleration at t>3.9s is equivalent to the

value of the wheel slip acceleration at t<2.3s. Traction loss, therefore, after t>3.9s cannot be determined by the wheel slip acceleration alone. The only metric that can be used to verify traction loss has occurred after 3.9s is by inspection of the wheel slip velocity. At steady state the wheel slip velocity equates to the angular acceleration, $\alpha = \omega$. With wheel slip velocity equating to the angular velocity and the wheel slip acceleration being approximately zero demonstrates that the system is in pure slip and traction loss has transpired.

Traction loss, therefore, can be estimated using the neighborhood N. The neighborhood, however, does not provide quantitative data representing traction loss like the derivative of the slip curve, though it does provide a qualitative representation of traction loss. Traction loss does not occur at t=2.3s but traction loss is occurring by 3.9s. Within this neighborhood the relative ground velocity has reached a maximum at approximately 2.9s, and is near zero at 3.9s. The displacement and the force also reach steady state by 3.9s. The neighborhood, therefore, provides only qualitative data representing when traction loss is occurring.

Figure 17-21 represent comparable experimental results for the test conducted on sand. For the experiments conducted in sand, the neighborhood N can still be defined. The two vertical lines define a neighborhood N between 1.9 and 2.5s, Figure 17. The neighborhood occurred sooner and the breadth of the neighborhood was narrower on sand than it was on carpet. This was due to synergetic behavior of the tether force and the chosen terrain. Before 1.9s there was no linear displacement of the vehicle. The required static force to move the tether did not occur until after this point. After 1.9s the traction force was sufficient enough to allow the vehicle to move forward. Between 1.9s and 2.5s

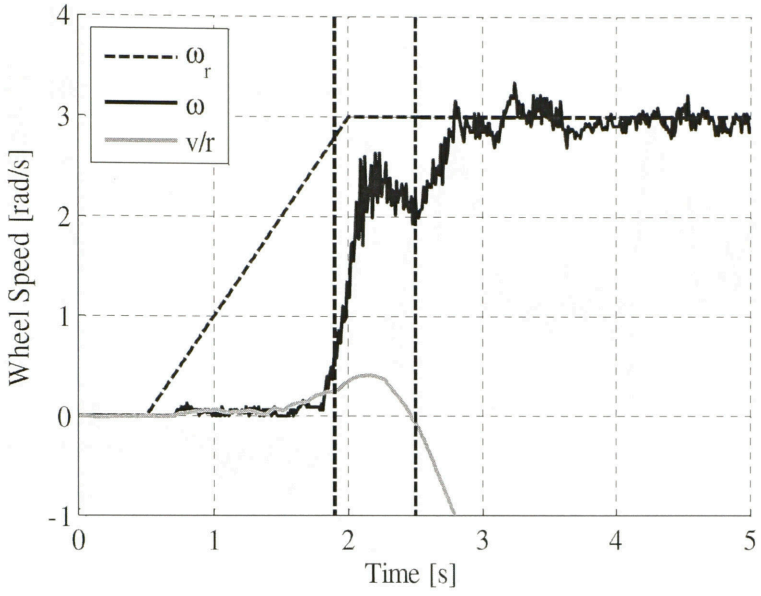

Figure 17: Comparable estimate of the wheel speed and relative ground velocity compared to the desired wheel speed reference for tests conducted on sand

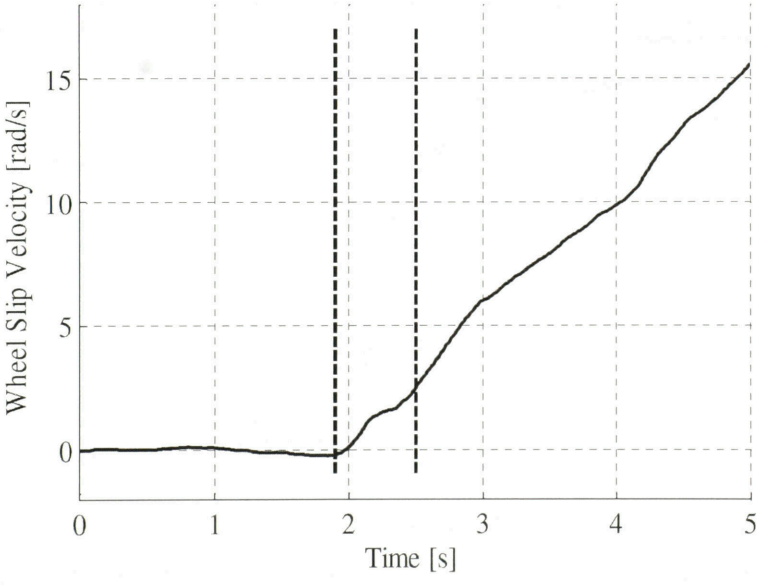

Figure 18: Comparable estimate of the wheel slip velocity for an experiment conducted on sand

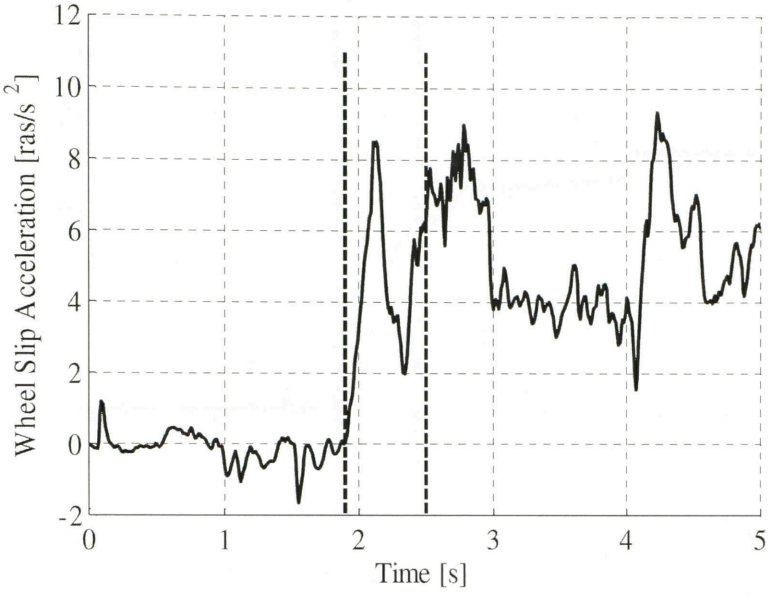

Figure 19: Comparable estimate of the wheel slip acceleration for experiments conducted on sand

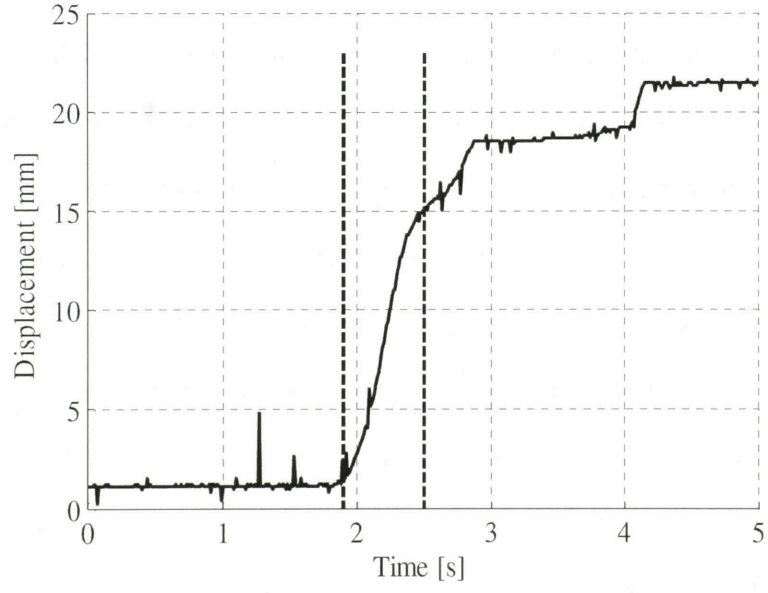

Figure 20: Comparable displacement of the linear potentiometer for experiments conducted on sand

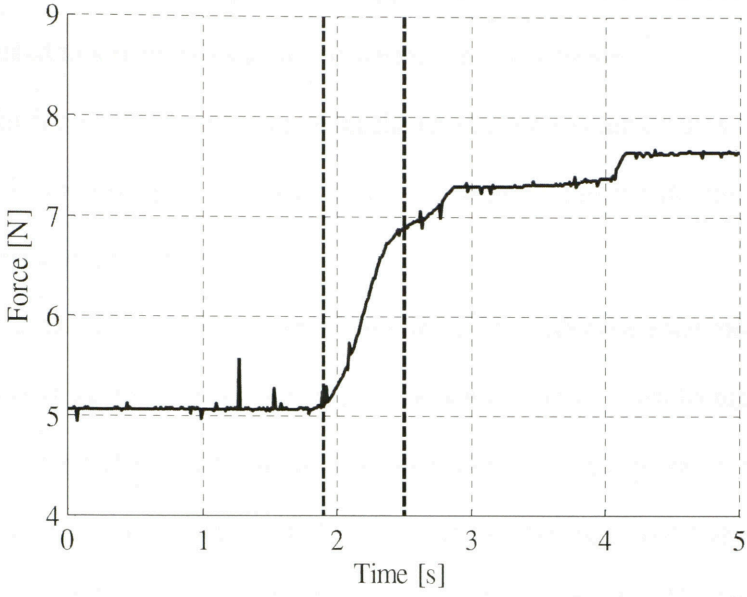

Figure 21: Comparable force acting on the linear potentiometer for experiments conducted on sand

the vehicle's displacement increased from zero to approximately 15mm. This limited travel shows that the chosen linear potentiometer for carpet was to stiff. A linear potentiometer with less stiffness, therefore, is required to allow the mobile robot to travel further. Although the tether force was too stiff, our traction estimation algorithm was able to quantify a region where traction loss was occurring.

In Figure 21 it can be seen that the forcing did not reach steady state at the upper limit of the neighborhood at t=1.5s as it did on carpet. The mobile robot after this point started to dig into the sand. At certain instances the robot dug sufficiently into the sand to produce enough torque to move the tether. This produced stair stepping in the force profile. The first stair step occurs at t=2.8s. Two others occur at 3.25s and 4.5s. Since the front wheels were digging into the sand the mobile robot tilted. The tilted caused a gravity bias error in the accelerometer. The relative ground velocity and the wheel slip.

velocity, therefore, were poorly defined. A poor estimate of the wheel slip velocity after 2.9s propagated to a poor estimate of the wheel slip acceleration

For a further investigation comparing the experiments conducted on carpet and sand, the appendix contains a broader spectrum of figures to aid in validating our proposed traction estimation algorithm.

By coupling the definition of wheel slip into a first order dynamic model of a vehicle we were able to circumvent an estimate of the wheel slip by introducing the wheel slip velocity. Allowing the wheel slip velocity and wheel slip acceleration to be estimated using onboard sensors, we were able to show a region where traction loss was occurring by defining a neighborhood bounded between to instances in time. The lower limit of this neighborhood was defined by a large increase in the wheel slip velocity, which corresponded to an increase in the wheel slip acceleration. The wheel slip velocity, therefore, is a useful tool for estimating traction loss in mobile robots that are constrained to operate at low wheel speeds. The wheel slip velocity and wheel slip acceleration can also be used as a tool for traction control. Since the foundation of the wheel slip velocity was framed upon a first order differential equation, we can utilize that equation to design a control law capable of bounding the wheel slip velocity and wheel slip acceleration.

4. TRACTION CONTROL OF A MOBILE ROBOT

4.1. Introduction

Using our traction estimation algorithm we propose a continuous robust controller that enforces an upper limit on the wheel slip velocity. Having an upper bound on the wheel slip velocity enables our control law to maximize traction.

A unique aspect of our traction controller is that it works jointly with a robust tracking controller. The tracking controller's purpose is to drive the angular velocity of the wheel to a desired reference. Since both controllers are robust, each works independently to reject unmodeled disturbances. When traction loss occurs, our proposed traction control law reduces the control input to a DC motor, which results in decreasing the overall wheel speed. Decreasing the overall wheel speed induces an error between the actual wheel speed and in the desired wheel speed reference. The robust tracking controller, therefore, attempts to drive the motors harder to attain the desired velocity. To alleviate both aforementioned controllers from fighting one another, our proposed traction control law is designed to work cooperatively with the tracking controller.

A representation of our proposed traction estimation and control system is provided in Figure 22. The output of the plant model provides measurement of the angular velocity, ω, from an optical encoder, and a measurement of the acceleration, a, using an accelerometer. The angular velocity signal is sent to our proposed robust tracking controller to determine the control input, ψ, required to follow the predetermined

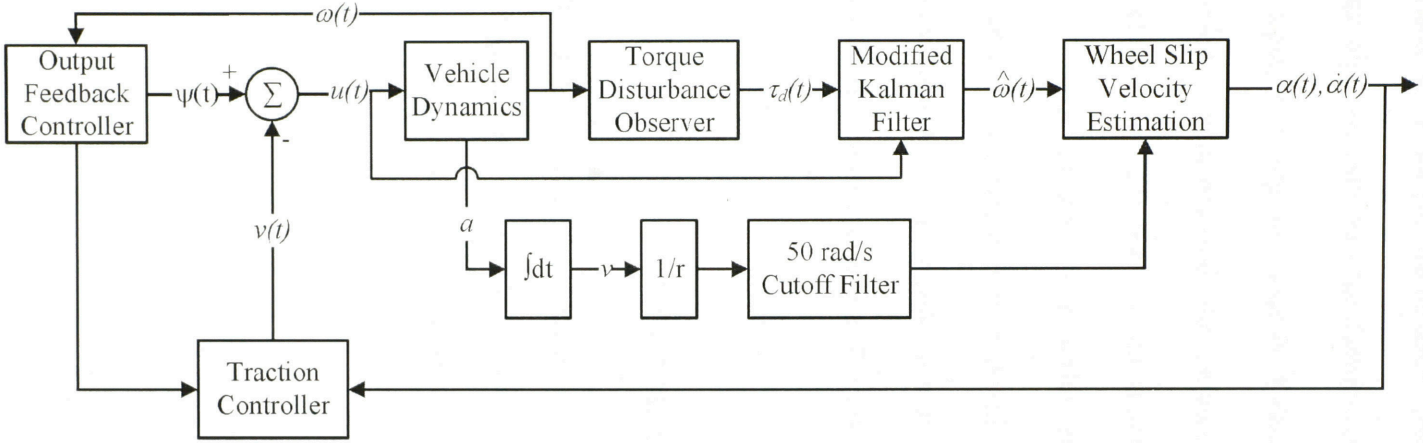

Figure 22: Block diagram representing our cooperative tracking and traction controllers

trajectory. The angular velocity signal is also fed indo our modified Kalman Filter, which is comprised of a torque disturbance observer and a Kalman Filter. The torque disturbance observer estimates the disturbance torque, τ_d, using the angular velocity and the plant input, τ. Using our modified Kalman Filter we obtain a better estimate of our angular velocity data, $\hat{\omega}$. Both the estimate of the angular velocity and the relative ground velocity, *v/r*, are sent to our traction estimation algorithm. The wheel slip velocity, α, from our traction algorithm and the control input, ψ, from our robust tracking controller are used by our proposed robust traction controller. The control input, *v*, from our proposed traction controller and the control input, ψ, from our proposed tracking controller are then summed. The resultant is the control input to our plant model, τ.

4.2. Traction Control Design

4.2.1. Robust Tracking Control Design

To design a traction controller, a control law must first be derived to drive a DC motor. Assume the dynamics of a wheel of a mobile robot follow the general state equation

$$\begin{aligned} \dot{x}_1 &= x_2, \\ \dot{x}_2 &= -\frac{\hat{B}}{\hat{J}} x_2 + \frac{1}{\hat{J}} \tau, \\ y &= x_1, \\ \left|\hat{B}\right| &\le \hat{B}_{\max}, \left|\hat{J}\right| \le \hat{J}_{\max}, \end{aligned} \quad , \tag{30}$$

where x_1 is the angular position of the wheel, x_2 is the angular velocity of the wheel, and $\hat{B}$ and $\hat{J}$ are estimates of the bounded mechanical damping and inertia of the wheel. The goal is to design a controller that tracks a position reference, r, and robustly rejects parameter uncertainty.

To track the reference, the states of equation (30) are transformed into error coordinates where

$$\begin{aligned} \mathbf{e} &= [e_0 \quad e_1 \quad e_2], \\ e_0 &= \int x_1 - \theta_r, \\ e_1 &= x_1 - \theta_r, \\ e_2 &= x_2 - \dot{\theta}_r, \end{aligned} \tag{31}$$

Taking the derivative of equation (31) yields

$$\begin{aligned} \dot{e}_0 &= e_1, \\ \dot{e}_1 &= e_2, \\ \dot{e}_2 &= -\frac{\hat{B}}{\hat{J}} e_2 + \frac{1}{\hat{J}} \tau - \ddot{\theta}_r, \end{aligned} \tag{32}$$

Let τ take the following form

$$\tau = \phi + v, , \tag{33}$$

where ϕ is a feedback linearization controller whose purpose is to stabilize the origin of equation (31) and v is a robust controller that compensates for parameter uncertainty. The control input then becomes,

$$\tau = -\hat{J}\left(-\frac{\hat{B}}{\hat{J}}x_1 + s - \ddot{r}\right) - \beta \tanh\left(\frac{3s}{e}\right),, \tag{34}$$

where s is the sliding manifold,

$$s = K_0 e_0 + K_1 e_1 + e_2, \tag{35}$$

and K is designed to make equation (32) stable and guarantees the an error convergence on the surface when s=0 shown in equation (34). The robust gain, β, can then be solved where

$$\beta \geq \frac{\left|K_0 e_1 + K_1 e_2\right|\left|1 - \frac{\hat{J}}{J}\right| + \left|\ddot{r}\right|\left|1 - \frac{\hat{J}}{J}\right| + \left|\delta\right|\left|\frac{B}{J} - \frac{\hat{B}}{\hat{J}}\right| + \left|x_2\right|\left|\frac{B}{J} - \frac{\hat{B}}{\hat{J}}\right|}{\frac{1}{\hat{J}}} = \rho(x), \tag{36}$$

It can be shown that this proposed control law stabilizes the tracking problem given in equation (32).

4.3. Traction Control Design

To provide a mobile robot the ability of maximizing traction, there must be a certain degree of wheel slip. In this section we propose a continuous Lyapunov Redesign controller [16], which will confine the wheel slip velocity, α, to a neighborhood. The size of the neighborhood is dependent on the control gain of the continuous controller.

As a part of our proposed traction estimation algorithm, we derived a wheel slip velocity estimator, which is defined as

$$\dot{\alpha} = -\frac{\hat{B}}{\hat{J}}\alpha + \frac{1}{\hat{J}}(\tau - Fr). \tag{37}$$

where τ is the applied wheel torque and F is the traction force defined through Pacejka's Tire Model, and α is the wheel slip velocity and is defined as

$$\alpha = \omega - \frac{v}{r}, \dot{\alpha} = \dot{\omega} - \frac{\dot{v}}{r}. \tag{38}$$

Equation (38) defines the wheel slip velocity as being an error state between the angular velocity of the wheel and the relative angular velocity of the vehicle. To derive a control law based upon equation (37) a function has to be defined that models the traction force applied to the wheel slip model.

A proposed function can be derived using the causal relationship from Pacejka's Tire Model. Pacejka's Tire Model places two constraints on the wheel slip, which helps facilitate the type of constraints required for the wheel slip velocity. The first constraint is the wheel torque, which is proportional to the traction force when the wheel slip is zero. Similarly, the wheel torque is proportional to the traction force when the wheel slip velocity is zero. The second constraint derived from Pacejka's Tire Model is determined when the wheel slip is unity. During pure slip the linear momentum of the vehicle stagnates despite having wheel torque. The wheel torque, therefore, does not correlate to the traction force. Likewise, our traction estimation algorithm also has to provide an upper bound on the wheel slip velocity, which will correlate to having no wheel torque mapped to the traction force. Quantifying an upper bound on the wheel slip velocity is difficult to ascertain since the wheel slip velocity is an error state. The functional

relationship between the traction force and the wheel slip velocity, however, is valid and can be summarized by the following:

$$F = g(\alpha)\frac{\tau}{\hat{J}r}, 0 < g(\alpha) < 1, \tag{39}$$

where $g(\alpha)$ is a smooth, bounded function that approaches zero at some upper bound of the wheel slip velocity. The purpose in defining the forcing in (39) is to allow an ideal mapping between the wheel torque and the traction force when $g(\alpha)$ is unity and no mapping between the wheel torque and the traction force when $g(a)$ is zero. For simplicity it is assumed $g(\alpha)$ is a decaying exponential equation that can model the prescribed constraints where

$$g(\alpha) = e^{-a|\alpha|} \tag{40}$$

In this equation a acts as a pseudo time constant, which dictates how quickly it will asymptotically approach zero. The pseudo time constant a can, therefore be adjusted to model the relationship between the wheel torque and the traction force. Applying equation (40) to equation (37) modifies the traction estimation function to

$$\dot{\alpha} = -\frac{\hat{B}}{\hat{J}}\alpha + \frac{1}{\hat{J}}\left(1 - g(\alpha)\right)\tau. \tag{41}$$

Implementing this substitution makes the wheel slip velocity estimator strictly a function of the wheel slip velocity and the wheel torque, which allows us to formulate a control law that will mitigate traction loss by bounding the wheel slip velocity. A discontinuous control law will first be defined, which will robustly drive the wheel slip velocity to zero.

Making the control law continuous, however, will attempt to drive the wheel slip velocity to zero, but it will be shown that our control law is only capable of bounding the wheel slip velocity. Our objective, therefore, is to determine the necessary control gains to minimize the neighborhood on the wheel slip velocity and maximize our ability to track a desired angular velocity reference.

Assume the wheel torque can be defined as follows

$$\varphi = \tau + v\,, \tag{42}$$

where τ is the control input to stabilize the tracking problem of equation (34), and v is the control input to stabilize equation (41). Substituting this control law into equation (41) gives,

$$\dot{\alpha} = \frac{\hat{B}}{\hat{J}}\alpha + \frac{1}{\hat{J}}\left[1 - g(\alpha)\right](\tau + v)\,. \tag{43}$$

Given this general equation for traction estimation, the robust tracking control input τ can be viewed as a known, bounded disturbance to the system. The control design problem then becomes one of providing a control law v to stabilize the system under this disturbance. To achieve this, the control law needs to dominate the disturbance.

To derive a control law that will dominate over the disturbance generated from the robust tracking controller, consider the Lyapunov candidate function,

$$V = \frac{1}{2}\alpha^2\,. \tag{44}$$

Taking the derivative of equation (44) gives

$$\dot{V} = \alpha\dot{\alpha} = \frac{\hat{B}}{\hat{J}}\alpha^2 + \frac{\alpha}{\hat{J}}\left[1 - g(\alpha)\right](\tau + v) \tag{45}$$

To stabilize the system, the derivative of the Lyapunov candidate function must be negative definite.

To accomplish this, let

$$v = -\eta\frac{w}{|w|}, \tag{46}$$

where η is the robust gain and w is the control variable, which are defined as,

$$\begin{aligned} &\eta \geq \frac{\rho}{1-k_0}, \\ &|\tau| + \delta|v| \leq \rho + k_0|v|, . \\ &w = \frac{\alpha}{\hat{J}}\left[1 - g(\alpha)\right], \end{aligned} \tag{47}$$

Substituting the control law into equation (45) produces

$$\begin{aligned} \dot{V} &\leq -\frac{\hat{B}}{\hat{J}}\alpha^2 - \eta\frac{w^2}{|w|} + |w||\tau|, \\ &\leq -\frac{\hat{B}}{\hat{J}}\alpha^2 - \eta|w| + \eta|w|, -\frac{\hat{B}}{\hat{J}}\alpha^2, \end{aligned} \tag{48}$$

which shows the derivative of the Lyapunov function is negative definite in the neighborhood $N = \{\alpha \in R\}$. This control law guarantees the stabilization of the system under the bounded disturbance τ.

This controller, however, drives the wheel slip velocity to zero. According to Pacejka's Tire Model, to maximize traction force there has to be a degree of wheel slip,

which correlates to a degree of wheel slip velocity. We, therefore, desire to drive the wheel slip velocity to a neighborhood. To accomplish this, we provide a continuous controller,

$$v = -\eta \tanh\left(\frac{3w}{\varepsilon}\right), \tag{49}$$

where ε is some tuned parameter. The gain of three is in the numerator to allow the hyperbolic tangent to approximately equal one when $w = \varepsilon$, Figure 23. This figure displays the effects of ε on equation (49) assuming the robust gain, η, is unity.

By deriving the nonlinear controller in equation (49) the command derived from the tracking controller can be robustly rejected. By setting the robust gain, $\eta = \tau$, allows perfect cancellation of the command derived from the tracking controller as the

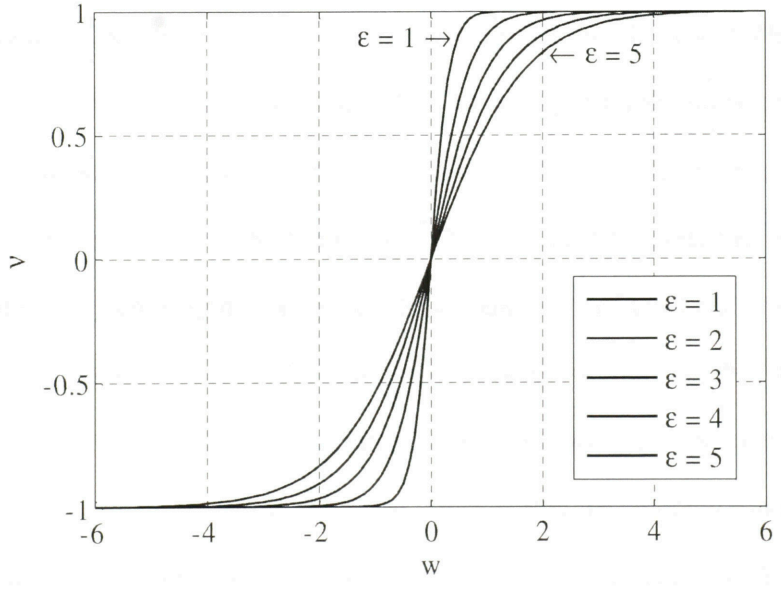

Figure 23: Effects of the ε on the control output, ν, with a unity robust gain, η

hyperbolic tangent approaches unity. Increasing the robust gain on the traction controller, $\eta > \tau$,results in mitigating the command derived from tracking controller for smaller values of the wheel slip velocity, α. Decreasing the robust gain, $\eta < \tau$, reduces the magnitude of the command from the tracking controller and does not cancel out the command.

Another feature of our proposed traction controller is its ability to cooperate with our proposed tracking controller. Our proposed controller in equation (49) has an embedded switching element allowing the controller to effectively null its command for small magnitudes of the wheel slip velocity. In the derivation of our proposed traction controller we provided an exponential function in equation (45) to account for the interaction between force and torque as a function of the wheel slip velocity. This same function us is used to determine the control variable, *w*, in equations (47) and (49). For large values of the wheel slip velocity, α, the control input asymptotically approaches $\alpha / \hat{J}$, and effectively turns on the controller. As the wheel slip converges to zero, the control input, *w*, approaches zero, which effectively turns off the traction controller allowing command from the tracking controller to drive the system unhindered.

Since the control law is continuous, the system will converge to a bounded neighborhood. By converging the system to a bounded neighborhood simply means the controller will attempt to drive the wheel slip velocity to zero, but this ideal state may never be reached. Since the proposed control design is stable, an upper and lower limit on the wheel slip velocity, therefore, will exist. Once within the neighborhood, the nature of the controller will confine the wheel slip velocity within the upper and lower limits. To estimate the range of this neighborhood, the continuous control law must be substituted

into the Lyapunov candidate function. Performing this operation modifies the Lyapunov function to

$$\dot{V} \le -\frac{\hat{B}}{\hat{J}}\alpha^2 + \frac{\varepsilon(1-k_0)}{4} \le -\frac{\hat{B}}{\hat{J}}\alpha^2 + \frac{\varepsilon}{4}, k_0 = 0. \tag{50}$$

The surface where $\dot{V} = 0$ defines an estimate of the contour defining the boundary of the neighborhood. The boundary of the neighborhood, which defines the convergence of the continuous controller, is

$$\frac{\hat{B}}{\hat{J}}\alpha^2 \le \frac{\varepsilon}{4}. \tag{51}$$

Only through implementing our continuous traction controller in experimentation can the actual size of the neighborhood be defined. Equation (51), however, does explain a certain aspect of the size of the neighborhood. As the value of ε increases the size of the neighborhood also increases. This will be verified through experimentation.

In the design of our control law, we have the ability to compensate for traction loss and to dominate over the robust tracking controller. The traction controller has also been designed to be continuous and ensure the system will converge within a defined neighborhood. When traction loss is not prevalent, this control law will be small compared to the robust tracking controller. The robust tracking controller will then dominate the system and will track the desired reference.

4.4. Experimental Setup

4.4.1. Methods and Procedures

The traction control law was evaluated in experimentation using a single axis mobile robot. A representation of the experimental setup is explained in Section 3.6. The same experimental setup from this section was followed since it worked well for providing tests with repeatable wheel slip. Since our traction control law is based upon the wheel slip velocity, this experimental setup established a foundation to prove the efficacy of our traction controller.

The tracking control law and the traction control law were evaluated using the algorithm provided in equations (34) and (49). Tests were conducted on carpet, which offered a surface with ample traction force. First, experiments were conducted on carpet without the tether and without the traction control law. The purpose of this was to determine the control gains for the tracking controller. Once the tracking controller provided acceptable results on carpet without the tether, tests were conducted with the tether. The control gains for the tracking controller were then modified to robustly reject the disturbance from the tether.

The traction control law was then implemented on the robot with the tether. The purpose of the experiments was to determine the balance necessary to effectively dominate over the tracking controller when traction loss occurs. To accomplish this certain parameters were modified. These parameters included varying the size of the continuous envelope, ε, and the dominance of the robust gain, η, from equation (49). To evaluate the performance of the proposed tracking/traction controller, several tests were conducted. The performance of the controller was dependent on its ability to converge

within the desired neighborhood by evaluating α and evaluating the maximum force, F, and maximum displacement, Δx. With each control gain, several tests were conducted to acquire sufficient statistical data to determine how the system reacted under these gains.

4.5. Experimental Results and Discussion

4.5.1. Robust Nonlinear Sliding Mode Tracking Controller

The control gains for the robust tracking controller were determined through experimentation on a single axle mobile robot. A linear potentiometer whose stiffness produced a force as function of the displacement of its chord provided an ideal unknown disturbance to the mobile robot. For experimental purposes it was our desire to adjust the control gains such that the vehicle followed a straight course. The gains of the controller were modified experimentally until the response of the system followed the desired course. Using the control gains K=[400, 40], ε=.1, and $\beta = 1.2\rho(x)$ the mobile robot was able to adequately transverse in a straight course.

The tracking of the reference velocity, however, was not accurate, Figure 24, 25. As can be seen from the figure the gains for the right wheel were able to adequately follow the desired trajectory. The gains for the left wheel, however, were not able to adequately follow the desired trajectory. This was a result of not optimizing the control gains for the left wheel. If time permitted, the control gain for the left wheel would have been adjusted to drive the left wheel to the desired trajectory. However, the nonoptimal gains for the left wheel produced a unique challenge for the proposed traction controller since the time profile of the wheel slip for the left wheel and right wheel were different, Figure 26, 27.

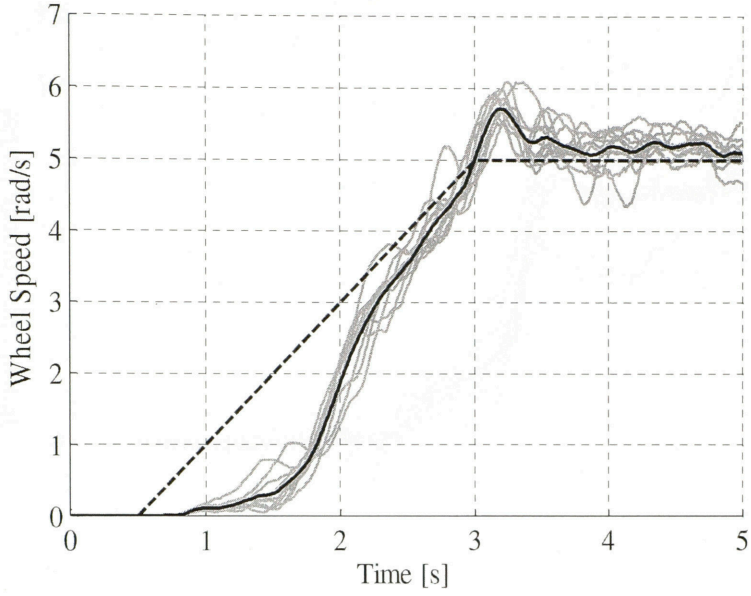

Figure 24: Dynamic response of the right wheel compared to the reference wheel speed implementing our proposed robust traction controller

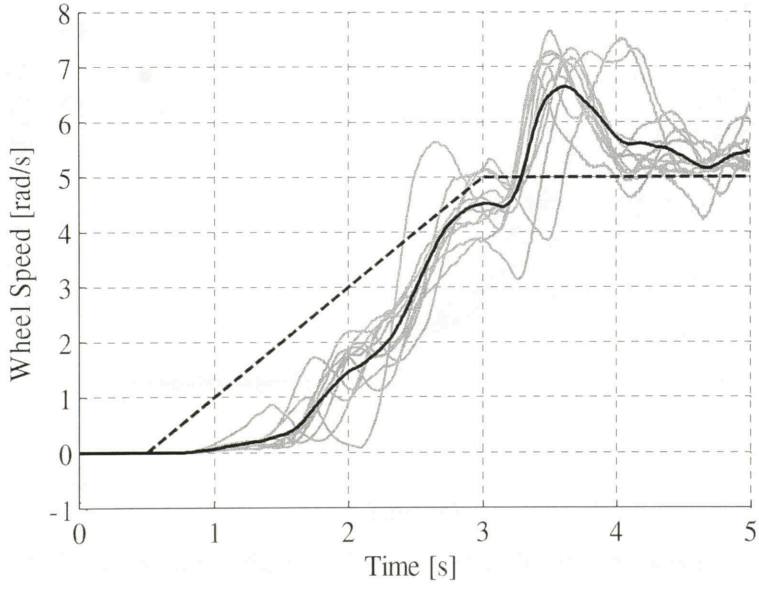

Figure 25: Dynamic response of the left wheel compared to the reference wheel speed implementing our proposed robust traction controller

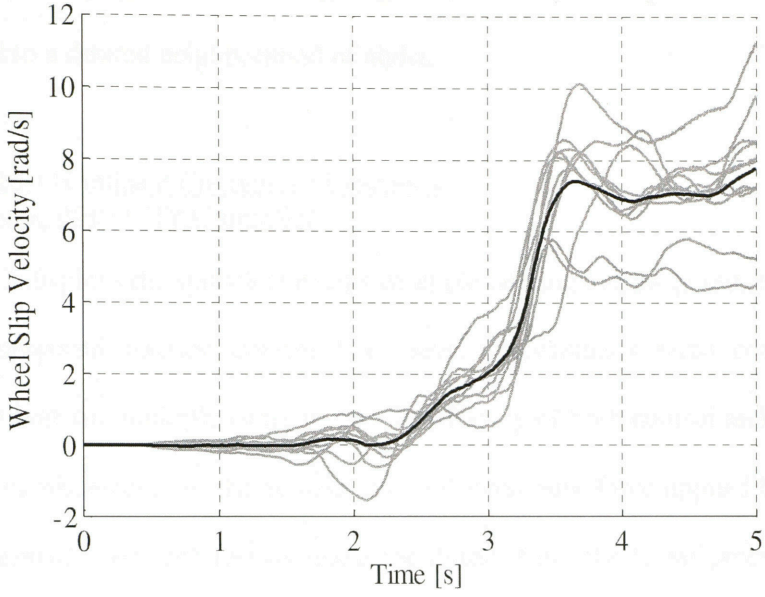

Figure 26: Estimate of the wheel slip velocity for the right wheel

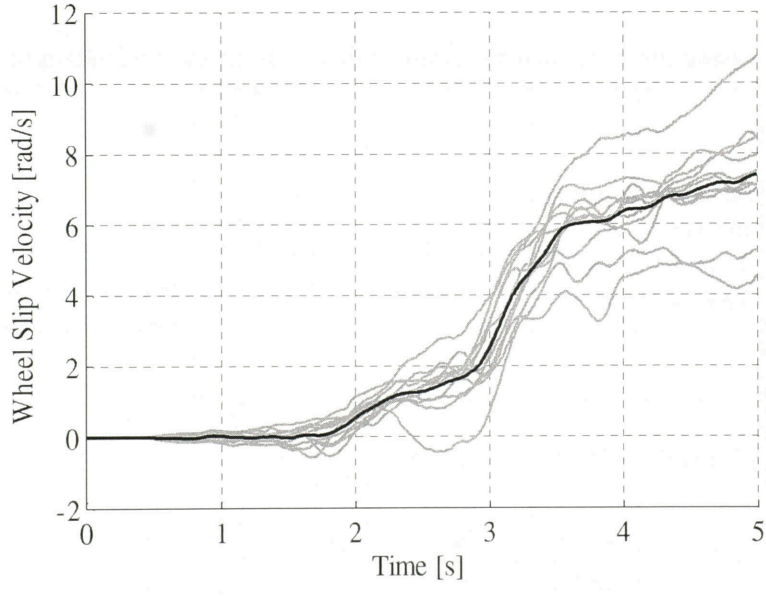

Figure 27: Estimate of the wheel slip velocity for the left wheel

Validation of our proposed traction algorithm is proven by driving both the left wheel and right wheel to a desired neighborhood of alpha.

4.5.2. Robust Nonlinear Continuous Lyapunov Redesign Wheel Slip Controller

Table 2 displays the statistical results of implementing our proposed tracking control law and proposed traction control law. Seven experiments were conducted. Each experiment was run multiple times to test the efficacy of both control architectures. The maximum displacements of the vehicle, Δx, and maximum force applied by the vehicle, F, were estimated for each test by using the output from the linear potentiometer. The maximum relative ground velocity of the vehicle, v/r, and the average steady state value for the wheel slip velocity, α, were post processed using the accelerometer and encoder

Table 2: Statistical results of the traction controller with different gains

No.	Traction Controller	Number of tests	Traction Controller Gains			Displacement	Average Steady State Force	Maximum Relative Ground Velocity	Average Steady State Wheel Slip Velocity	
									α (rad/s)	
			ε	a	η	Δx (m)	*F* (N)	*v/r* (rad/s)	Front Right	Front Left
1	On	11	5	-0.2	1.2	0.30	24.78	2.72	1.95	1.71
2		11	2		1	0.26	22.85	3.37	0.63	0.58
3		11	3		1	0.26	22.53	3.09	0.68	0.40
4		11	1		1	0.21	19.67	2.99	0.41	0.34
5		11	5		1	0.24	21.61	2.13	2.45	1.90
6		11	4		1.2	0.26	22.80	2.55	1.86	1.56
7	Off	11	-	-	-	0.26	22.70	2.64	6.89	7.39

signals.

Experiments 1-6 were conducted using both the proposed robust tracking control law and the proposed robust traction control law using different values for ε and the robust gain, η. The value of ε was investigated to determine an upper bound on the convergence of the wheel speed velocity. The robust gain was also modified to determine an appropriate value that would dominate over the robust tracking controller. Experiment 7 was conducted with the traction controller off. This experiment, therefore, only incorporated the tracking controller to regulate the vehicles wheel speed. Experiment 7 represents the baseline test to compare the effectiveness of our proposed traction control law. This test provides an appropriate comparison for the convergence of the wheel slip velocity and the maximum displacement of the vehicle. Implementing our proposed traction controller, regardless of the value of ε or the robust gain, the wheel slip velocity was able to be controlled and was bounded. From Table 2 the steady state wheel slip velocity for the baseline test was approximately 7 rad/s. The maximum steady state wheel slip velocity obtained using our proposed traction controller only reached 2.5 rad/s. The convergence of the wheel slip velocity for each test, however, is difficult to obtain using the statistical results alone. The table only represents the average steady state wheel slip velocity. An investigation into our proposed robust traction controller, therefore, will be shown using the results from experiment 5.

One of the main benefits of our proposed traction controller was its ability to cooperate with our tracking controller. Figure 28 displays the response of the angular velocity of the front right wheel using the traction control gains $\eta = 1$ and $\varepsilon = 5$. The response of the angular velocity is presented in grey, while the time average of the wheel

speed is presented in black. The dashed line represents the reference angular velocity the tracking controller was commanded to follow. At the beginning of the experiment the vehicle is stationary and the wheel slip velocity is zero. The wheel slip velocity, therefore, is at the origin of the bounded neighborhood. From this time on the traction controller will attempt to keep the vehicle within a bounded neighborhood. As can be seen from the figure there is an apparent maximum in the wheel speed velocity at 3.0s. Before 3.0s the tracking controller is dominating the system. The vehicle therefore is commanded to follow the reference trajectory. At 3.0s the wheel slip velocity has reached 2rad/s. The traction force, therefore, is reaching a maximum, Figure 29. At this instance the traction controller begins to dominate over the tracking controller. The reduction in the wheel speed between 3.0 and 3.5s demonstrates that the traction controller is continuing to increase its dominance over the tracking controller. By 3.5s the angular velocity of the wheel has reached an average of 1.5 rad/s, the wheel slip velocity has reached a steady state response of 2.5rad/s, and the traction force has reached a maximum of approximately 22N. The steady state response of the wheel slip represents the upper limit of the bounded neighborhood of the wheel slip velocity. The traction controller, therefore, is dominating over the tracking controller and will keep the wheel slip velocity at this upper limit. We have, therefore, provided a traction controller capable of cooperating with a tracking controller. Using these control gains, our traction controller was also shown to keep the wheel slip velocity within a bounded neighborhood whose upper limit was 2.5rad/s. In order to decrease the upper limit of the wheel slip velocity, the control gain, ε, must be decreased.

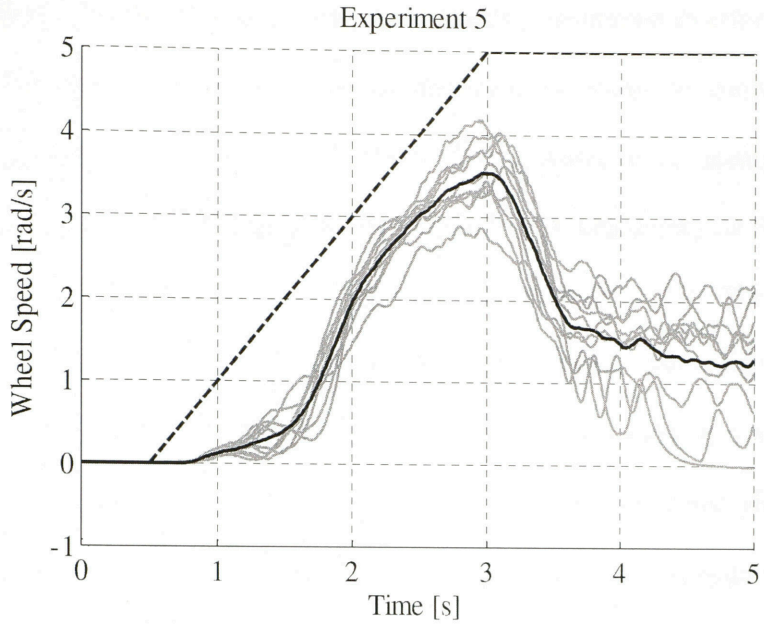

Figure 28: Wheel speed variation of the right wheel for experiment 5; results (grey), mean results (solid black), wheel speed reference (dashed)

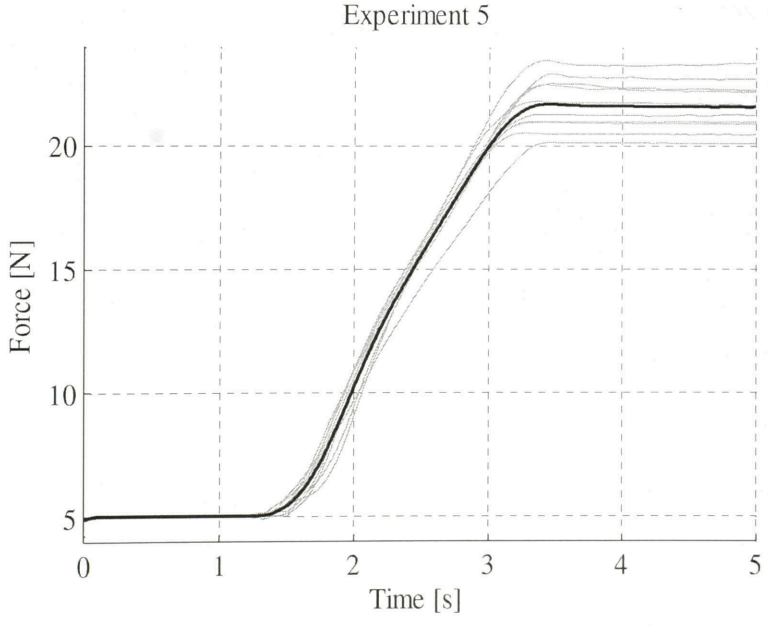

Figure 29: Force acting on the linear potentiometer versus time for experiment 5

The effects the control gain, ε, were investigated to determine its effects on the upper bound on the wheel slip velocity and to determine its ability to cooperate with our proposed tracking controller. Larger values of ε resulted in an appropriate balance between the traction and tracking controller, Figure 30-35. Depending on the value of ε the steady state wheel slip velocity varied between 2-2.5 rad/s. The robust gains, however, affected the upper bound on the wheel slip velocity. This is depicted in Figure 30, 34, 35. For each of these tests the value of ε remained constant at 5 while the robust gain, η, was decreases from 1.2 to 1. For a robust gain, η=1, the wheel slip velocity was bounded to an average of 2.45 while a robust gain of η = 2 reduced the wheel slip velocity to 1.95. Larger robust gains, therefore, mitigate the command from the tracking controller by robustly rejecting its command, which resulted in reducing the upper bound on the wheel slip velocity. The optimal robust gain for ε, however, was not determined experimentally due to time constraints. Determining the optimal robust gains for any value of ε is a subject of future work.

As the value of ε was decreased, however, the dispersion of the wheel slip velocity increased and created oscillations in the wheel slip velocity, Figure 31-33. This occurred due to the switching element derived in the traction controller. Recall the switching element between the two controllers is the exponential equation (40), which represent mapping between the wheel slip velocity and the percentage of wheel torque converted to forward motion. At steady state the smaller values of ε resulted in increasing the oscillatory behavior of the wheel slip velocity. This was due to the increased frequency of switching between the two controllers at steady state. Since increasing the robust gain for

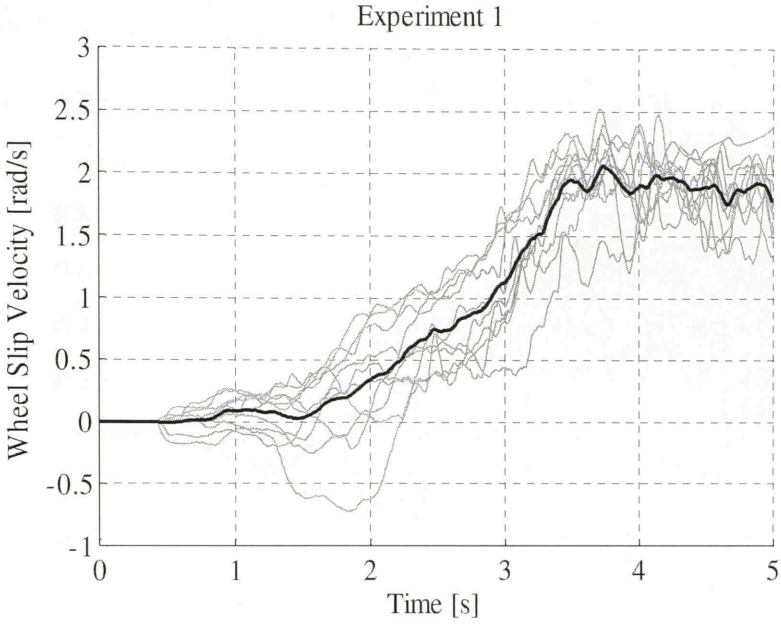

Figure 30: Right wheel slip velocity variation for experiment 1

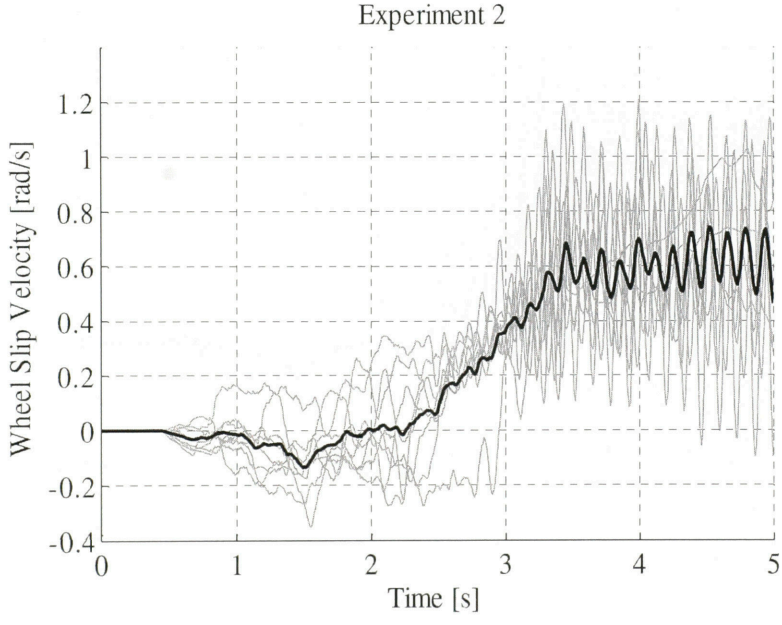

Figure 31: Right wheel slip velocity variation for experiment 2

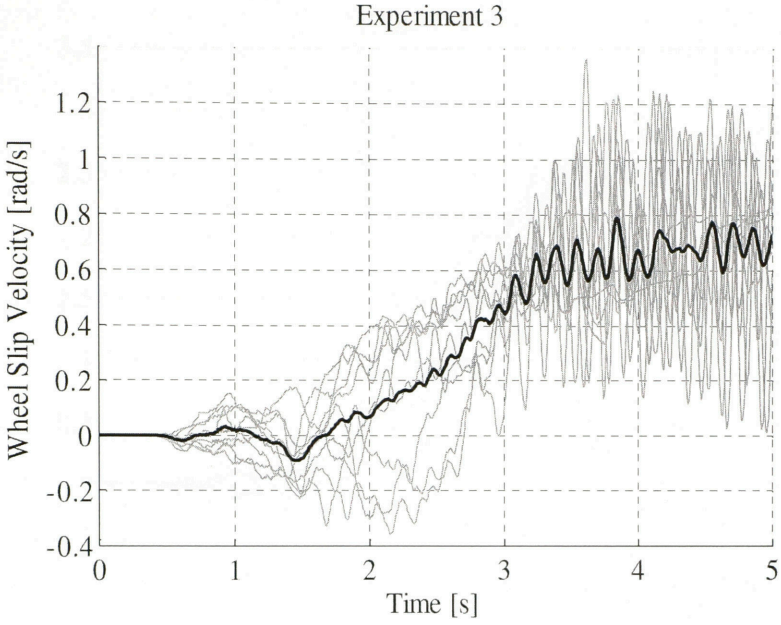

Figure 32: Right wheel slip variation for experiment 3

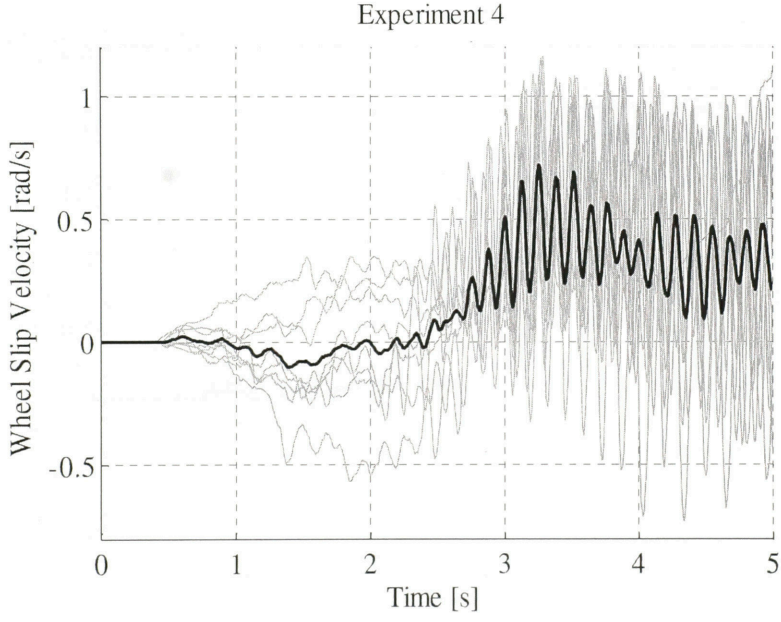

Figure 33: Right wheel slip velocity variation for experiment 4

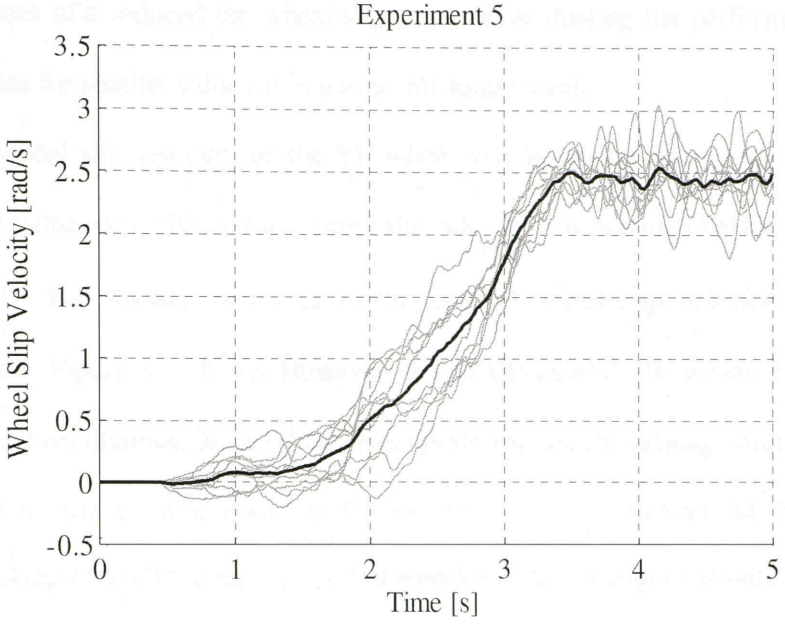

Figure 34: Right wheel slip velocity variation for experiment 5

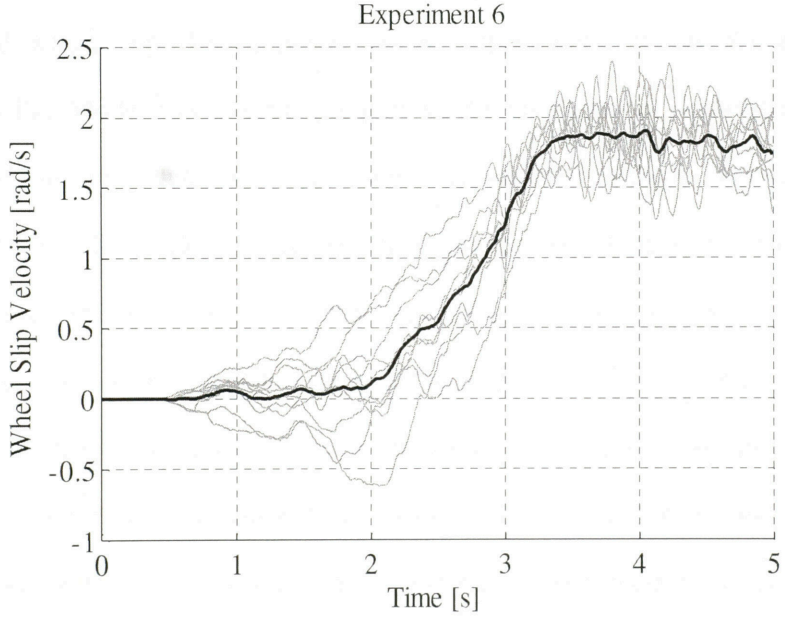

Figure 35: Right wheel slip velocity variation for experiment 6

larger values of ε reduced the wheel slip velocity, evaluating the performance in larger robust gains for smaller values ε is a topic for future work.

The wheel slip velocity for the left wheel too shows similar results, Figure 36-41. For Large values of ε, the average wheel slip velocity was bounded below 2 rad/s, Figure 36, 40, 41. For smaller values of ε, the average wheel slip velocity was bounded below1rad/s, Figure 37, 40, 41. However, for all values of ε, the steady state wheel slip velocity had oscillations. Recall that the gains for the robust tracking controller were not optimized for the left wheel. Due to the switching element between the controllers, the larger tracking controller gains for the left wheel resulted in larger oscillation.

For mobile robot applications where the relative ground velocity, *v/r*, are small the wheel slip velocity provides a better quantitative estimate of traction loss than using the traditional wheel slip. Using postprocessed experimental results for experiment 5, Pacejka's Tire Model was estimated, Figure 42. In this figure the experimental results are represented in grey while the mean result is represented in black. The wheel slip was estimated using the single axis accelerometer and the optical encoder. An estimate of the traction force was generated from the linear potentiometer. As can be seen from the figure, the wheel slip increases sharply between 5N and 6N. To better understand the effects of estimating Pacejka's Tire Model using wheel slip for low speed applications, one of the runs from experiment 5 was isolated. Figure 43 displays an estimate of the wheel slip as a function of time for the second run of experiment 5. As can be seen from the figure, the wheel slip increased sharply between 0.6 and 1.6s and reached a local maximum of 0.9 at approximately 0.86s. This time segment corresponds to the initial acceleration of the vehicle. During this time segment, small differences between

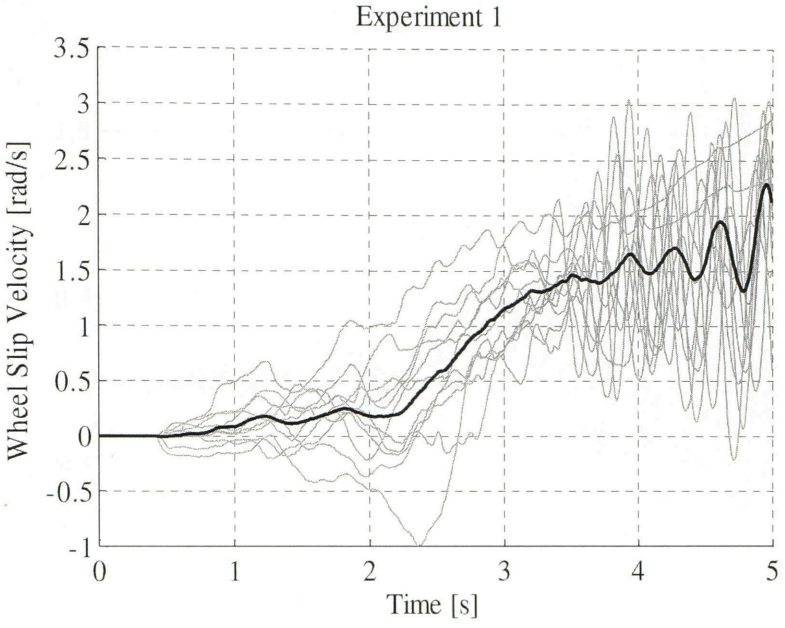

Figure 36: Left wheel slip velocity for experiment 1

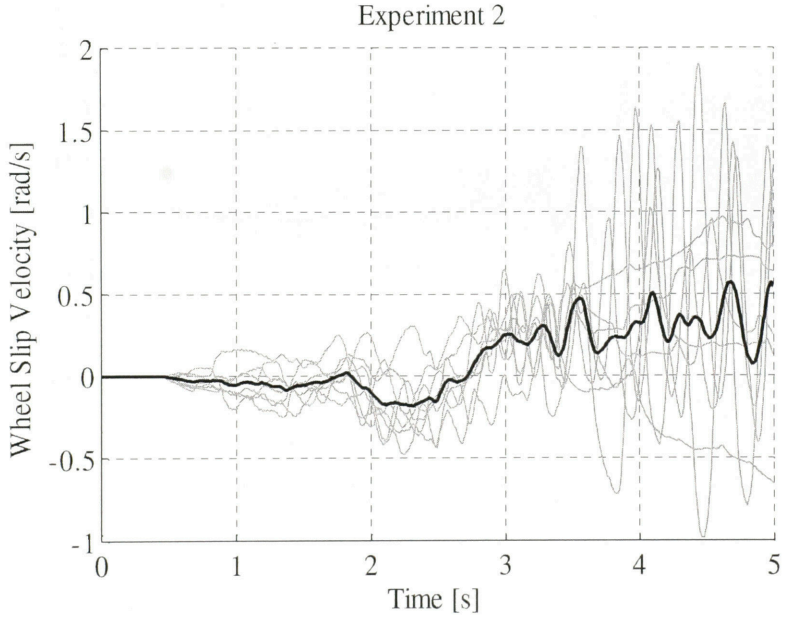

Figure 37: Left wheel slip velocity for experiment 2

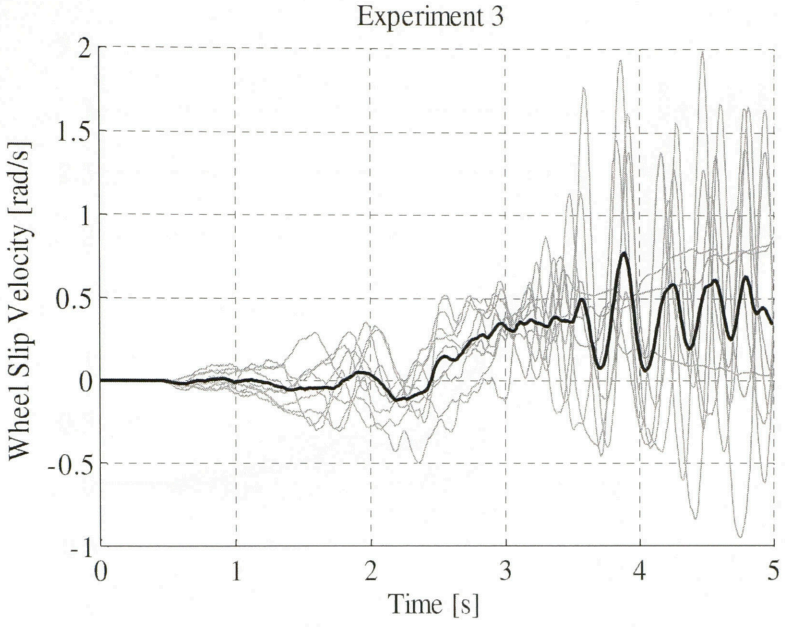

Figure 38: Left wheel slip velocity for experiment 3

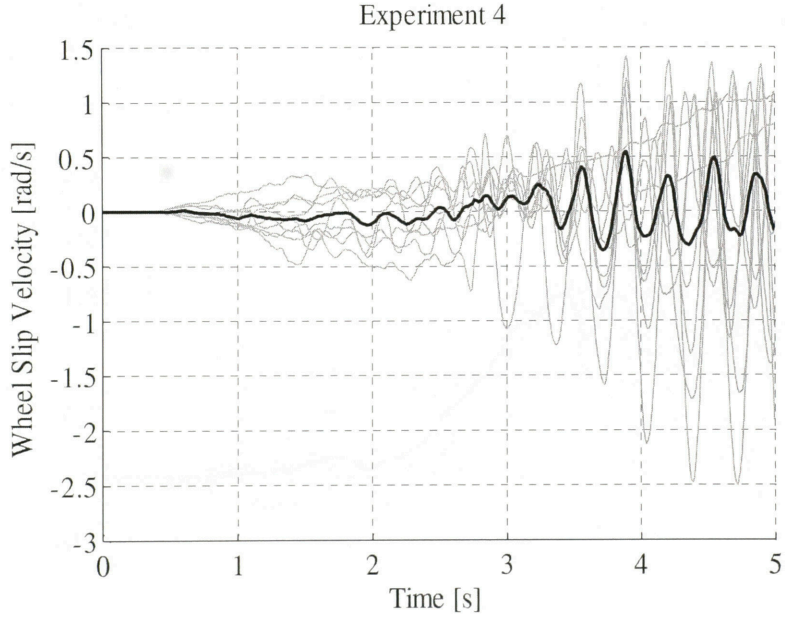

Figure 39: Left wheel slip velocity for experiment 4

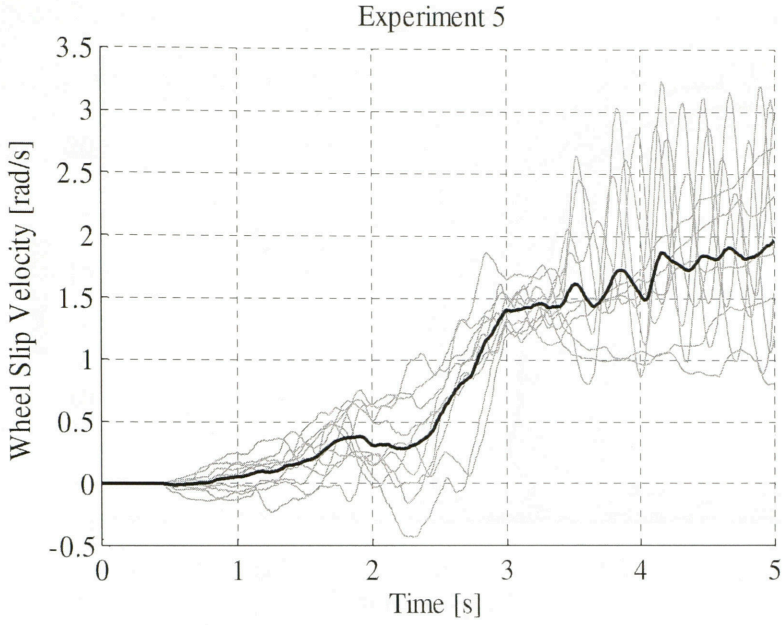

Figure 40: Left wheel slip velocity for experiment 5

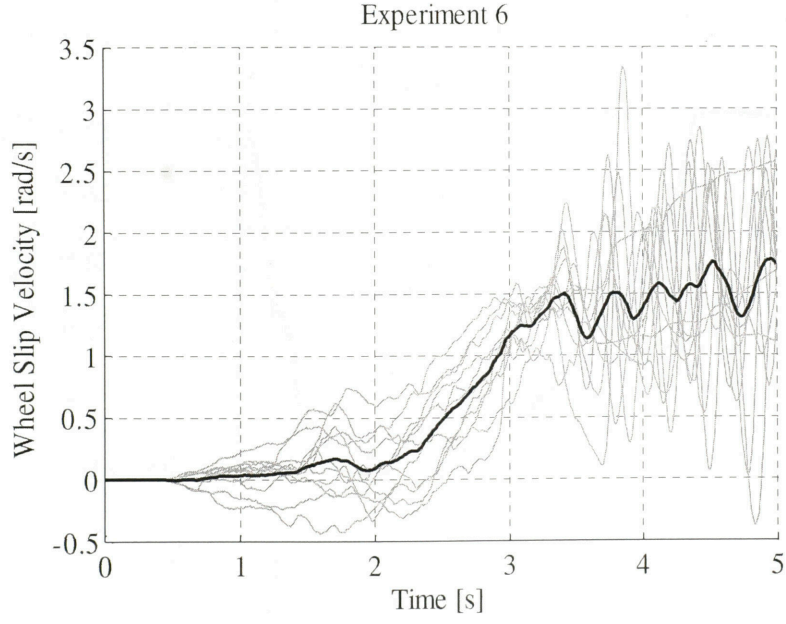

Figure 41: Left wheel slip velocity for experiment 6

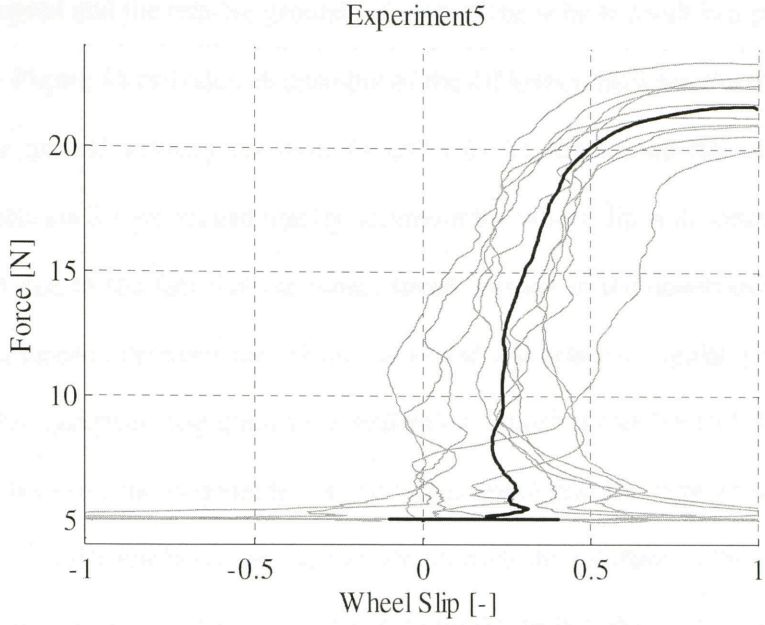

Figure 42: Estimate of Pacejka's Tire Model for experiment 5

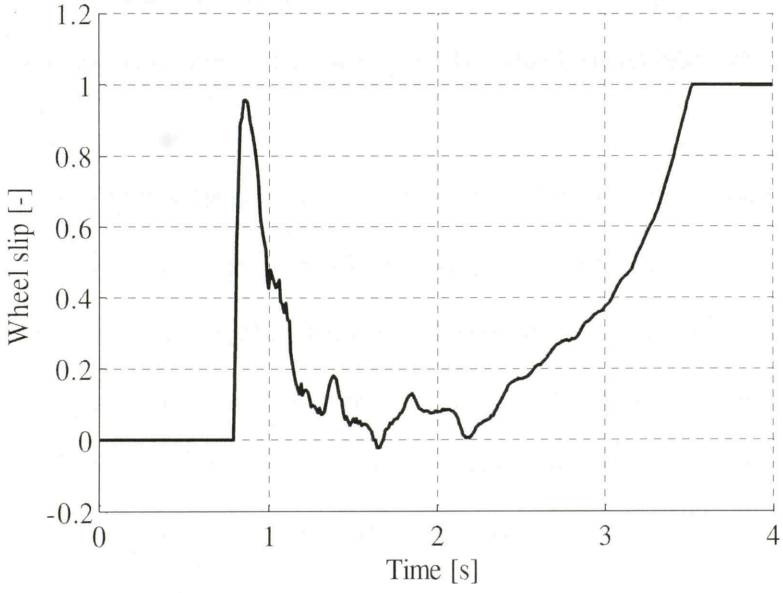

Figure 43: Estimate of the wheel slip versus time for experiment 5 run 2

the wheel speed and the relative ground velocity of the vehicle result in a poor estimate of wheel slip. Figure 44 provides an example of the difference between the wheel speed and the relative ground velocity between .6s and 1.6s for the second run of experiment 5. Recall in Section 2.1 we argued that by definition the wheel slip is ill suited for low speed application due to the fact that the wheel speed appears in the denominator of equation (2). The difference between the wheel speed and the relative angular velocity is small from at 0.86s and their magnitudes are well below .1rad/s. From 0.9 to 1.2s, however, the difference between the magnitudes of the wheel speed and the relative angular velocity has increased sufficiently enough to provide an accurate estimate of the wheel slip. The wheel slip in this region of time is reduced from 0.9 to 0.2. When the magnitudes of the wheel speed and the relative linear velocity are small the estimate of the wheel slip is poorly defined. Using the estimate of the wheel slip velocity at low speed, however, is not effected by small differences between the wheel speed and the relative angular velocity.

Figure 44 displays the estimate of the wheel slip velocity between 0.6 and 1.6s. Recall by definition the wheel slip velocity is a pure error states; i.e., the error state does not require any complex mathematical operations besides addition and subtraction. The wheel slip velocity, therefore, is not prone to division by zero like wheel slip or is small. The figure shows that between 0.6 and 1.6s the wheel slip velocity did not become undefined or was poorly estimated when the wheel speed was small. The wheel slip velocity resulted in estimating the error between the wheel speed and relative ground velocity. The wheel slip velocity, therefore, was not affected by small differences

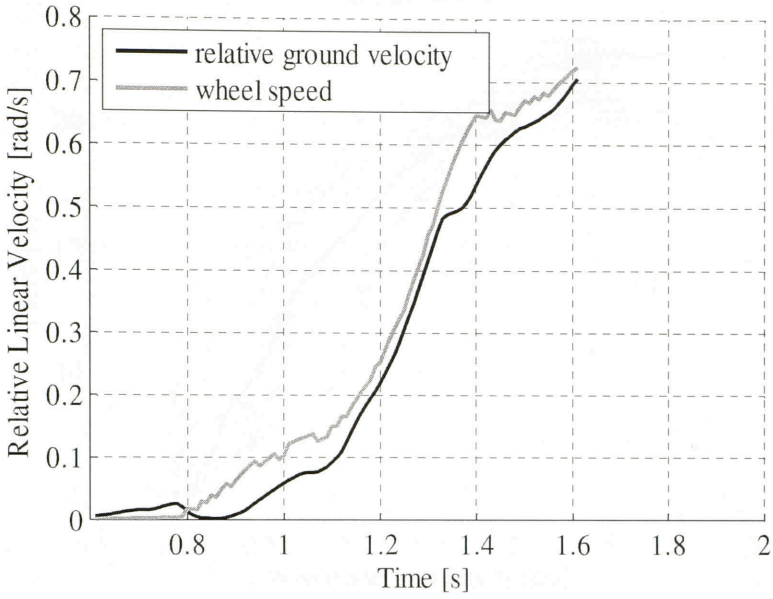

Figure 44: Estimate of the relative ground velocity compared to the Kalman filtered wheel speed for experiment 5 run 2

between the wheel speed and relative ground velocity. Recognizing that the wheel slip velocity should be used for low speed applications, the wheel slip velocity, therefore, can be used to estimate Pacejka's Tire Model.

Figure 45 represents an estimate of Pacejka's Tire Model using the wheel slip velocity. Recall, one of the major characteristics in Pacejka's Tire Model is that the initial slope of the curve is positive. An initial increase in the traction force, therefore, corresponds to an initial increase in wheel slip. Likewise, an initial increase in traction force should correspond to an increase in the wheel slip velocity. As can be seen from the figure, there is no large change in the wheel slip velocity between 5N and 6N, unlike utilizing wheel slip. The wheel slip velocity, therefore, captured the initial slope of Pacejka's Tire Model whereas using the wheel slip did not. An increase in the wheel slip velocity, therefore, corresponded to an increase in the traction force. Another

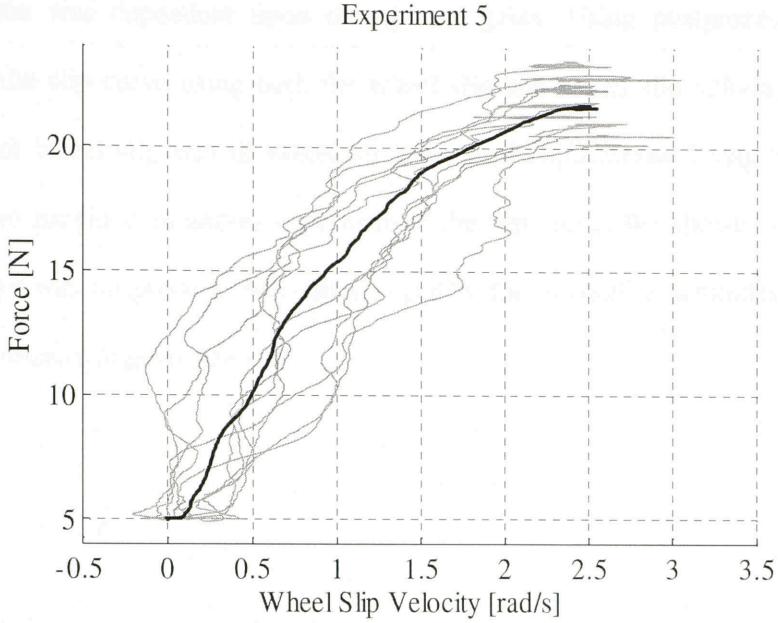

Figure 45: Estimate of Pacejka's Tire Model using the wheel slip velocity for experiment 5

characteristic of Pacejka's Tire Model is that there is maximum reachable traction force. As can be seen from the figure a maximum in the slip curve is reached. The figure, however, does not appear to show a decrease in traction as the wheel slip velocity increase. Future work will entail developing a better estimate of the slip curve. The major purpose of these figures, however, was achieved. For low speed applications, it was shown that small magnitudes of wheel speed and linear velocity produce a poor estimate of the wheel slip. Using the wheel slip, therefore, did not correlate well with Pacejka's Tire Model. Using the wheel slip velocity, however, did result in a better estimate of Pacejka's Tire Model for low speed applications.

We have developed a robust control law capable of mitigating traction loss by controlling the wheel slip velocity. Using this control law, we showed that the robust traction controller was capable keeping the wheel slip velocity below an upper limit

whose value was dependant upon the control gains. Using postprocessed data, we estimated the slip curve using both the wheel slip and wheel slip velocity. Our results showed that wheel slip was ill suited for low speed applications. Using the wheel slip velocity, we provided an alternate estimate of the slip curve. We showed that the wheel slip velocity was no prone to becoming ill posed due to small magnitudes of the wheel speed and relative angular velocity.

5. CONCLUSION AND FUTURE WORK

5.1. Traction Estimation

We have derived a new algorithm that replaces the estimation of wheel slip with the wheel slip velocity. It was first shown that the wheel slip velocity can be observed using a first order differential equation that couples the dynamics of the wheel with the dynamics of the vehicle. Further investigation of the wheel slip velocity resulted in defining the wheel slip velocity and wheel slip acceleration as measurable error states. Using the wheel slip velocity and wheel slip acceleration, we were able to define a region where traction loss is occurring.

To achieve an accurate estimate of the wheel slip velocity and wheel slip acceleration, we designed a modified Kalman Filter. The system model describing the dynamics of the wheel is augmented by introducing an estimate of the unmodeled torque disturbance.

To validate our traction estimation algorithm, an output feedback controller was designed to produce repeatable wheel slip by following a prescribed velocity trajectory in the presence of a tether. Providing experiments with repeatable wheel slip resulted in allowing us to estimate the wheel slip velocity and its derivative in a controlled manner. By estimating the wheel slip and wheel slip acceleration, we were able to show that traction loss was confined to a neighborhood bounded by two instances in time as described in Figure 12-15.

Fusing the data from the modified Kalman Filter with the data from the single axis accelerometer, we showed that traction loss was detectable in a neighborhood. Experiments conducted on carpet provided a surface that resulted good estimates of our traction estimation variables α and $\dot{\alpha}$. Through the good estimates of α and $\dot{\alpha}$, a neighborhood was clearly defined when traction loss was occurring. A neighborhood defining when traction loss transpired was also observable with the tests conducted on sand. Sand, however, provided a surface that stressed the limits of our traction estimation algorithm.

Gravity bias drift, however, caused poor estimation of the relative angular velocity for experiments on soft terrain. The gravity bias drift occurred from the mobile robot digging into the sand. With the mobile robot digging into the sand, the robot tilted and modified the angular component of gravity, which resulted in changing the gravity bias of the accelerometer. To compensate for the angular component of gravity we plan on replacing the single axis accelerometer with a three axis inertial measurement unit (IMU). By incorporating an IMU on the mobile robot, the gravitational components of acceleration can be estimated. The gravitational components can, therefore, be backed out of the response of the IMU and a better estimate of the vehicles acceleration can be achieved. Providing an IMU on the vehicle also introduces the ability of modeling terrain topography.

Digging of the mobile robot is not the only terrain characteristic that can cause the gravity bias of the accelerometer to change due to the angular component of gravity. Rarely in an actual environment will the terrain be hard and perfectly parallel to the local horizontal. A particular path may include a change in the topology of the environment.

The topology of the environment will cause the mobile robot to pitch and roll, which will change the bias of the accelerometer. The gravity vector can also provide knowledge of the vehicles orientation, which assists in decomposing the topography of the environment.

The experiments on sand also introduced the necessity of using a different linear potentiometer. Since the available traction was less on sand than carpet, the linear potentiometer dominated over the available traction on the sand. This resulted in the robot moving only ~35mm for the duration of the experiment. To provide a better test setup on sand, or other terrains where traction is low, a linear potentiometer with a lower force profile should be used. We are hopeful this will result in a similar displacement/force curve as on carpet.

To further validate our traction estimation, experimentation on multiple surfaces needs to be explored. Estimating acceleration through the (IMU) should allow multiple surfaces to be explored like gravel and rocks. Having a variety of linear potentiometers will allow testing upon surfaces with low traction.

The torque disturbance observer also opens research to be conducted on estimating the terrain characteristics. This can be accomplished by introducing a controller in the torque disturbance observer that attempts to drive the system to estimate motor parameters and unknown terrain characteristics by fusing the output from an observer derived from the wheel slip differential equation. Providing the terrain characteristics will result in the ability of measuring the slope of the slip curve since both the traction and wheel slip velocity will be known for each wheel. Providing that ability to control the

slope of the slip curve for each wheel will provide the ability of maximizing traction for each wheel.

By knowing the traction forces acting on each wheel a controller also can be designed, which provides the ability of following a desired path in the presence of traction loss. For example, assume one wheel can provide only a certain amount of traction to aid in the forward progression of the vehicle. The other wheels, using the slope of the slip curve, have the ability of providing more traction. Commands can, therefore, be given to the other wheels to drive the robot in a particular direction. Thus, to follow a desired path, the independently driven wheels should work cooperatively using the available traction provided by each wheel.

5.2. Traction Control

For low speed applications, we have proposed a robust traction controller that works jointly with a tracking controller to maximize traction forces by containing wheel slip velocity to a neighborhood. Unlike previously designed controllers that drive wheel slip ratio to a desired reference, our control law confines the wheel slip velocity to a neighborhood. Confining the wheel slip velocity to a neighborhood gives liberty of keeping the wheel slip velocity bound to a desired value. Our results show that when traction is available the wheel slip velocity is kept near zero. When more traction was required, our traction controller allowed the wheel slip velocity to increase. When traction was not available our traction controller reduced the wheel slip velocity to an upper limit whose value depended upon controller gains.

Utilizing the results from our traction controller we are able to show that for low speed applications the wheel slip velocity is superior to using wheel slip. Wheel slip was

sensitive to small differences between the linear velocity and relative linear velocity of the vehicle when the wheel speed was small. The wheel slip velocity was shown to not be sensitive for small wheel speeds.

Using the wheel slip velocity we showed that the wheel slip velocity produced a better estimate of the slip curve than using the traditional wheel slip for low speed applications. This is unique in that slip curves are generally defined using wheel slip. For low speed applications we showed that the characteristics of the slip curve were preserved. These characteristics include the heuristics defined for Pacejka's Tire Model. However, evidence of using the wheel slip velocity for estimating Pacejka's Tire Model was constrained to experiments conducted on carpet. Further testing on a variety of surfaces needs to be conducted to further validate our claim of using the wheel slip velocity for estimating the slip curve.

Though the robust control gains for experimentation were considered to be constant, the robust control gain should be investigated to see if the robust gains can be tuned in real time using the sliding manifold. Therefore, the robust gain is only as large as it needs to keep the wheel slip bounded.

Our approach in combining our traction controller and our tracking controller, however, may not have been the best method. Recall the voltage input to the motor is the summation of the tracking controller input and the traction controller input. The robust gain in the traction controller effectively acts like a switching element. When the wheel slip velocity is low, the control input from the traction is small, thereby, allowing the tracking controller to dominate the voltage input to the motor. When the wheel slip velocity is high, the traction controller dominates over the tracking controller. In

experimentation, we showed this method worked well when a good estimate of the wheel slip was achieved. Another approach is to use the wheel slip velocity in an outer loop guidance method. The objective of this guidance method is to shape the desired input trajectory. If the wheel slip velocity is low, the desired input trajectory remains the same. If the wheel slip velocity is high, however, the desired input trajectory is shaped to mitigate traction loss. Providing an outer loop guidance method based upon the wheel slip velocity and an inner loop tracking controller, therefore, will remove issue of having cooperative controllers.

However, though the proposed control law was shown to cooperate with a tracking controller while mitigating traction loss other forms of control techniques should be investigates. Recall that since the wheel slip velocity and wheel slip acceleration are error states allows any linear or nonlinear feedback control design to be implemented.

Though experiments were limited to carpet, further testing on different surfaces is required to explore our proposed traction control law. Providing tests on a variety of surfaces will allow us to tune the control gains for different surfaces. Finding the control gains that maximize traction on these surfaces provides the ability of designing a control law that is capable of tuning the control gains to maximize traction for a variety of surfaces.

APPENDIX

SENSOR SPECIFICATIONS

Table 3: Sensor specifications

Miniature Position Transducer	Specification	Units
Manufacturer	Firstmark Controls	
Part #	160-1285-C8SS	
Type	5 turn, precision, hybrid	
Resistance	5.0	K omhs
Travel	1800.0	Degree
Supply current	12.0	mA max
Supply voltage	35.0	VDC max
Shock	100 g for 6ms	g
Vibration	10 to 2000 Hz at 15 g	Hz
Tension range	5 to 28	N
Accelerometer	Specification	Unit
manufacturer	Colibrys	
Part #	MS 7000	
Acceleration	10.0	g
Bias	<50	mg
Bias stability	<25	µg/degC
Scale factor	100.0	mV/g
Axis alignment	< 10	mrad
Resolution threshold	<4	mg
Bandwidth	0 to > 600	Hz
Resonant frequency	2.7	kHz
Noise	7 to <18(max)	mV/sqrt(Hz)
Encoder		
Manufacturer	US Digital	
Part #	E2-1024-250	
Supply current	55 to 57	mA
Output voltage		
Low	0.5 volts @ 8mA	Volts
High	2.0 volts @ -8mA	Volts
Resolution	1024.0	CPR
2 channel quadrature	Yes	
Cycle error		
Typical	3.0	^{o}e
Max	5.0	^{o}e

REFERENCES

[1] R. Mukherjee, M. A. Minor, and J. T. Pukrushpan, "Simple motion planning strategies for spherobot: a spherical mobile robot," presented at The 38th IEEE Conference on Decision and Control (CDC), Dec 7-Dec 10 1999, Phoenix, AZ, USA, 1999.

[2] X. Zhu, M. A. Minor, and S. Park, "Distributed robust control of compliant framed wheeled modular mobile robots," *Journal of Dynamic Systems, Measurement and Control, Transactions of the ASME*, vol. 128, pp. 489-498, 2006.

[3] K. Iagnemma and S. Dubowsky, *Mobile Robots in Rough Terrain: Estimation, Motion Planning and Control with Application to Planetary Rovers*: Springer-Verlad Berlin Heidenlberg, 2004.

[4] H. B. Pacejka and E. Bakker, "Magic formula tyre model," *Vehicle System DynamicsProceedings of the 1st International Colloquium on Tyre Models for Vehicle Dynamics Analysis, Oct 21-22 1991*, vol. 21, pp. 1-18, 1993.

[5] C. Unsal and P. Kachroo, "Analytic nonlinear observer-based design for antilock braking systems," *Proceedings of the SPIE - The International Society for Optical EngineeringMobile Robots XI and Automated Vehicle Control Systems, 20-21 Nov. 1996*, vol. 2903, pp. 22-33, 1997.

[6] K. R. Buckholtz, "Reference input wheel slip tracking using sliding mode control," *SAE Technical Paper Series, 2002-10-0301*, 2002.

[7] C. Canudas-de-Wit and R. Horowitz, "Observers for tire/road contact friction using only wheel angular velocity information," presented at The 38th IEEE Conference on Decision and Control (CDC), Dec 7-Dec 10 1999, Phoenix, AZ, USA, 1999.

[8] S. Kang, M. Yoon, and M. Sunwoo, "Traction control using a throttle valve based on sliding mode control and load torque estimation," *Proceedings of the Institution of Mechanical Engineers, Part D: Journal of Automobile Engineering*, vol. 219, pp. 645-653, 2005.

[9] J. Song and K. Boo, "Performance evaluation of traction control systems using a vehicle dynamic model," *Proceedings of the Institution of Mechanical Engineers, Part D: Journal of Automobile Engineering*, vol. 218, pp. 685-696, 2004.

[10] C. Unsal and P. Kachroo, "Sliding mode measurement feedback control for antilock braking systems," *IEEE Transactions on Control Systems Technology*, vol. 7, pp. 271-281, 1999.

[11] K. Chun and M. Sunwoo, "Wheel slip tracking using moving sliding surface," *Proceedings of the Institution of Mechanical Engineers, Part D: Journal of Automobile Engineering*, vol. 219, pp. 31-41, 2005.

[12] M. Tai and M. Tomizuka, "Robust longitudinal velocity tracking of vehicles using traction and brake control," presented at 6th International Workshop on Advanced Motion Control, Nagoya, Jpn, 2000.

[13] J. van der Burg and P. Blazevic, "Anti-lock braking and traction control concept for all-terrain robotic vehicles," presented at Proceedings of the 1997 IEEE International Conference on Robotics and Automation, ICRA. Part 2 (of 4), Apr 20-25 1997, Albuquerque, NM, USA, 1997.

[14] H. Dugoff, Francher, P.S and Segel, L., "An analysis of tyre traction properties and their influence on vehicle dynamic performance," *SAE Trans*, pp. 79, 341-366, 1970.

[15] L. Ojeda, D. Cruz, G. Reina, and J. Borenstein, "Current-based slippage detection and odometry correction for mobile robots and planetary rovers," *IEEE Transactions on Robotics*, vol. 22, pp. 366-378, 2006.

[16] H. K. Khalil, "Nonlinear systems," 3 ed: Prentice Hall, 2002.